INVESTIGATING THE ROLE OF STRIATAL SPINY PROJECTION NEURONS IN COMPULSIVE BEHAVIORS

by

Brittany Lynn Chamberlain

BS Neuroscience, BA History and Philosophy of Science, University of Pittsburgh, 2019

Submitted to the Graduate Faculty of

University of Pittsburgh in partial fulfillment

of the requirements for the degree of

Bachelor of Philosophy

University of Pittsburgh

2019

UNIVERSITY OF PITTSBURGH

DIETRICH SCHOOL OF ARTS AND SCIENCES

This thesis was presented

by

Brittany Lynn Chamberlain

It was defended on

March 22, 2019

and approved by

Dr. Susan Sesack, Department of Neuroscience, University of Pittsburgh

Dr. Aryn Gittis, Department of Neurobiology, University of Pittsburgh

Dr. Meaghan Creed, Department of Anesthesiology, Pain Center, Washington University

Thesis Advisor: Dr. Susanne Ahmari, Department of Psychiatry, University of Pittsburgh

INVESTIGATING THE ROLE OF STRIATAL SPINY PROJECTION NEURONS IN COMPULSIVE BEHAVIORS

Brittany Lynn Chamberlain, BS, BA

University of Pittsburgh, 2019

Obsessive compulsive disorder (OCD) is a chronic, severe mental illness that affects 2-3% of the world's population. In recent years, neuroimaging studies have consistently shown abnormal patterns of activity within corticostriatal thalamocortical (CSTC) circuits in patients with OCD and reported that effective treatment with selective serotonin reuptake inhibitors (SSRIs) normalizes aberrant CSTC activity. However, the mechanism of this effect is unknown.

Because it is difficult, if not impossible, to investigate cellular and circuit mechanisms in human subjects, our lab turns to translational mouse models. Using *Sapap3*-knockout (KO) mice, which display a compulsive grooming phenotype and corticostriatal abnormalities, we sought to determine the role of spiny projection neurons (SPNs) in mediating compulsive behavior and to uncover potential neural correlates of effective SSRI administration. Using novel *in vivo* calcium imaging technology, we observed overall striatal hyperactivity in *Sapap3*-KO mice at grooming-onset relative to wild-type (WT) littermates, an effect that is driven by increased recruitment of groom onset-activated SPNs. SSRI treatment reduced the compulsive grooming behavior of *Sapap3*-KOs and decreased the neural correlate of this behavior, the percent of groom onset-activated SPNs observed in *Sapap3*-KOs.

To investigate the contributions of individual striatal subpopulations to the overall striatal hyperactivity observed in *Sapap3*-KOs, we used a double-transgenic strategy to generate D1-cre x *Sapap3*-KO and D1-cre x *Sapap3*-WT mice. Contrary to our predictions, we observed a

significant reduction in activity of D1-SPNs in *Sapap3*-KOs relative to WT mice. Following 7 days SSRI treatment, the compulsive grooming phenotype of D1-cre x *Sapap3*-KO mice was significantly reduced, but only minor changes in D1-SPN activity were observed. These findings suggest that D2-SPNs may be responsible for driving grooming-associated striatal hyperactivity in *Sapap3*-KO mice. While additional research is necessary to attain a more comprehensive understanding of the corticostriatal abnormalities in this translational model, the present findings provide clinically-relevant insights into the circuit level mechanisms underlying compulsive behaviors and the mechanisms by which SSRI treatment effectively reduces them.

Table of Contents

List of Schematics

List of Figures

ACKNOWLEDGEMENTS

I would like to acknowledge the many individuals who have supported and inspired me throughout this process. To all members of the Ahmari lab that I have had the privilege to learn from and work alongside, I thank you for allowing me to become a fully-fledged member of this incredible team. You have taught me that the difficult questions are the ones worth answering, and by your example, I have learned how to persevere in the face of any obstacle that comes my way.

In particular, I would like thank Sean Piantadosi for his guidance and encouragement over the past three and a half years. Thank you for answering every question I threw your way with patience and for teaching me how to "think like a scientist." I feel fortunate to have contributed to your graduate studies, and I eagerly look forward to seeing your future successes.

I would like to thank Dr. Susan Sesack of the Department of Neuroscience for sharing her knowledge and advice within the realm of neuroscience research and beyond. You challenged me to think critically and to push myself to achieve great ends. Above all, you believed in me in the moments when I was the most uncertain of my own abilities. For this, I am sincerely grateful.

Outside of academia, I would like to acknowledge my family and friends for their love and encouragement. To my friends: the college career path that we selected for ourselves has been demanding and trying at times. I am so fortunate that we have been able to lift each other up along the way. To my mother: thank you for instilling the importance of education in me at a young age and for always supporting my academic aspirations. My successes would not have been possible without your constant support.

Finally, I would like to express my gratitude to my thesis mentor, Dr. Susanne Ahmari. Your dedication to our lab's research is inspiring, and I thank you for granting me the opportunity

to pursue such valuable and rigorous research as an undergraduate student. Thank you for seeing my potential long before I could and for your continual guidance and encouragement over the past three and a half years. I hope to follow your example of excellence in my future as a physician scientist.

1.0 INTRODUCTION

1.1 Obsessive compulsive disorder

Obsessive compulsive disorder (OCD) is a chronic, severe mental illness that affects 2-3% of the world's population. OCD is characterized by two main symptom categories: intrusive distressing thoughts (obsessions) and repetitive behavioral acts (compulsions). This chronic disorder often begins in adolescence or early adulthood and can have an incredible impact on daily functioning and quality of life. Despite its severity and high prevalence, there is limited understanding of the precise mechanisms underlying OCD, and current treatment methods have limited efficacy.

1.1.1 Structural abnormalities in OCD

MRI studies that use voxel-based morphometry (VBM) to examine region-specific changes in gray matter volume have repeatedly reported significant volumetric alterations when comparing scans from OCD patients and healthy control subjects. In particular, studies report an increase in gray matter volume of the basal ganglia (Piras et al. 2015; Pujol et al. 2004; Rotge et al. 2009) and thalamus (Piras et al. 2015; Kim 2001; Christian et al. 2008; Rotge et al. 2009) in OCD patients relative to healthy controls. Additionally, several VBM studies have reported observing decreased gray matter volume in the anterior cingulate cortex (ACC) and orbitofrontal cortex (OFC) of OCD patients (Piras et al. 2015; Kim 2001; Van Den Heuvel et al. 2008). It is important to note that the results of structural MRI studies have been fairly heterogenous, with some studies reporting significant increases in cortical volume or decreases in striatal and thalamic volume. These

inconsistencies highlight our lack of understanding of the precise mechanisms that underlie structural changes in patients with OCD. To investigate these mechanisms further, it is necessary to examine how functional connectivity in corticostriatal thalamocortical (CSTC) circuits may be altered in OCD.

1.1.2 Functional abnormalities in OCD

Over the past two decades, mounting evidence has indicated that aberrant activity in CSTC circuitry may underlie OCD symptoms. fMRI and PET studies have repeatedly reported abnormal patterns of blood flow and glucose metabolism in CSTC regions in OCD patients. Specifically, at rest, glucose metabolism is increased in the OFC, ACC, and caudate nucleus of OCD patients compared to healthy control subjects (Graybiel and Rauch 2000; Saxena 1998; Menzies et al. 2008). Several studies have shown that this hypermetabolism is further accentuated upon symptom provocation by comparing glucose metabolism within subjects before and after showing a stimulus that has reportedly provoked OCD symptoms on previous occasions (Saxena 1998).

Effective treatment response appears to normalize metabolic rates in corticostriatal regions: in a group of OCD patients who received either serotonin reuptake inhibitors or cognitive behavioral therapy, glucose metabolism was significantly reduced in treatment-responsive individuals but not in nonresponders (Saxena 1999; Rauch 1994). fMRI studies have reported similar abnormal patterns of CSTC activation during symptom exposure that is normalized following effective treatment (Menzies et al. 2008; Breiter 1996). The correlation between normalization of corticostriatal activity and symptom reduction provides further evidence for the role of CSTC circuits in OCD pathophysiology.

Furthermore, fMRI studies can assess patterns of functional connectivity by performing seed-based cross-correlation analyses of subjects' resting-state imaging sequences. These studies have reported that patterns of functional connectivity between cortical and striatal regions are significantly altered in OCD patients compared to healthy control subjects. Specifically, one study reported that OCD patients had increased functional connectivity between ventral striatal regions (ventral caudate and putamen) and medial orbitofrontal cortex (mOFC) and that the strength of functional connectivity between ventral corticostriatal regions was predictive of symptom severity (Harrison et al. 2009). This finding was consistent with PET studies that report hypermetabolism in corticostriatal regions at baseline that is normalized with effective treatment and provides further support for the belief that CSTC circuit dysfunction underlies OCD pathophysiology (Burguiere et al. 2013).

1.1.3 Corticostriatal thalamocortical circuitry in OCD

It is well-established that the coordinated activity of the cortex, basal ganglia, and thalamus that comprise the CSTC circuit is pertinent for the execution of several cognitive and motor functions, including decision-making, action selection, and habit formation (Shepherd 2013; Pennartz et al. 2009). Given the symptomology of OCD (mental obsessions and behavioral compulsions), it is unsurprising that a wealth of structural and functional neuroimaging literature has implicated CSTC circuit dysfunction in the pathophysiology of the illness. The cortical regions of the CSTC circuit include the OFC, prefrontal cortex (PFC), and ACC, all of which have been implicated in motivation and determining reward preferences (Graybiel and Rauch 2000). The striatum integrates information from the cortex, thalamus, and midbrain regions to guide the selection of adaptive actions, projecting through basal ganglionic regions to the thalamus. In the final piece of the CSTC loop, the thalamus projects back to cortex, activating motor cortex such that the selected action is executed. Under normal conditions, then, CSTC circuitry guides progression from a cognitive framework, established in the cortex, to a corresponding behavioral output that is adapted based on this framework. It has been theorized that in OCD, dysfunction in CSTC circuits results

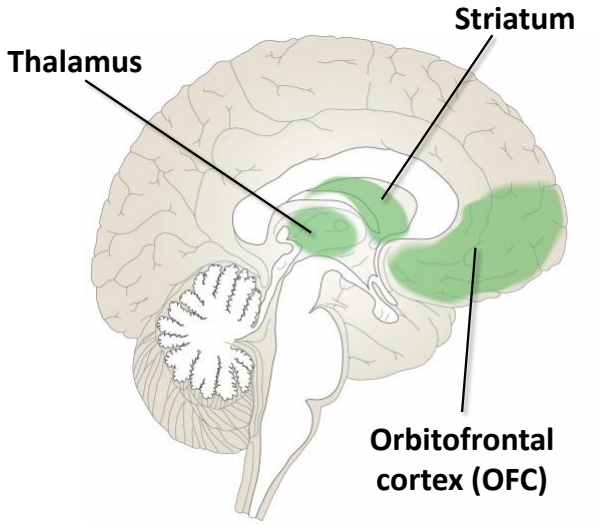

Schematic 1.1 Corticostriatal thalamocortical circuitry

Coordinated activity in the OFC, striatum, and thalamus give rise to decision-making, action selection, and habit formation. Neuroimaging studies implicate aberrant activity in these regions in the pathophysiology of OCD.

in patients becoming stuck in one cognitive framework, rendering them unable to transition to other behavioral outputs when a given behavior is no longer adaptive for their environment (Graybiel and Rauch 2000). This theory is commonly illustrated by considering an OCD patient with a contamination obsession. In this case, an anxiety-provoking stimulus may be seeing a cut on another person's hand, leading to subsequent feelings of distress over fear of a disease being carried through the air from the cut and infecting the patient. To seek relief from this distressing thought, the patient may perform a ritualistic behavior; in this case, excessive hand washing. Feeling momentary relief from their distressing thoughts, their compulsive behavior becomes reinforced, making it more probable that the patient will repeat this compulsive behavior the next time they encounter an anxiety-provoking stimulus (Pauls et al. 2014). This example is particularly insightful because it highlights that the ritualistic behaviors that OCD patients engage in are not inherently negative. Rather, the associated anxiety-relief that a certain behavior yields results in reinforcement of that behavior in a manner that becomes compulsive in nature over time.

1.1.3.1 Role of central striatum in adaptive action selection

The key locus of the CSTC circuit that is investigated in this study is the central striatum. The striatum receives input from sensory, motor, and associative cortices, and integrates these inputs to select adaptive motor programs for initiating goal-directed behaviors. The central striatum is composed of 95% GABAergic spiny projection neurons (SPNs) (Gagnon et al. 2017). SPNs can be further subdivided into two genetically-distinct subpopulations: dopamine 1 receptor- (D1-) and dopamine 2 receptor-expressing (D2-) cells.

D1-SPNs contain the amino acid substance P and the opioid peptide dynorphin and selectively project to the internal globus pallidus (GPi) and substantia nigra pars reticulata (SNr) (Surmeier et al. 2007). The GPi and SNr send inhibitory projections to the thalamus. Inhibition of the GPi and SNr by D1-SPNs in striatum disinhibits the thalamus, which then sends excitatory projections to the cortex, directing the execution of voluntary, goal-directed movements. In contrast, D2-SPNs contain enkephalin and selectively project to the external globus pallidus (GPe) (Surmeier et al. 2007). Rather than

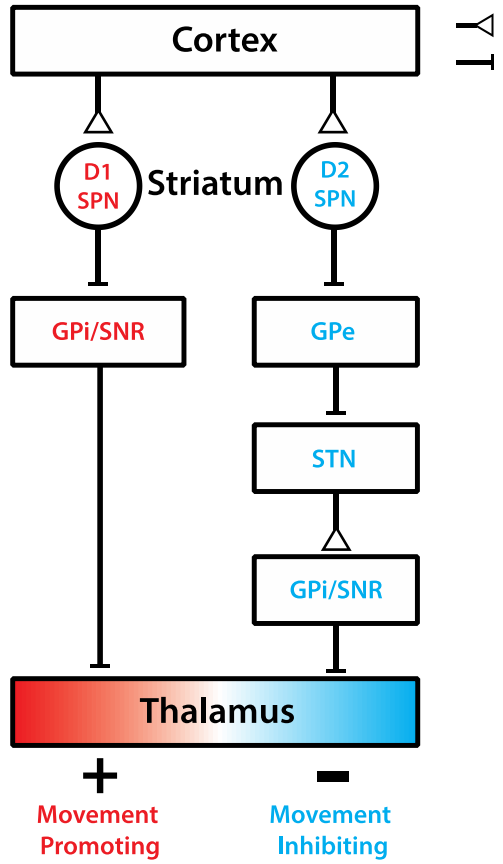

Schematic 1.2 Direct and indirect pathways of basal ganglia

The output structures of D1- and D2-SPNs diverge to make the direct and indirect pathways of basal ganglia. Through the direct pathway, D1-SPNs send inhibitory projections to GPi and SNr, disinhibiting the thalamus. Thalamus sends excitatory projections to cortex, directing initiation of desired movements. D2-SPNs send inhibitory projections to GPe, disinhibiting the GPi and SNr. When disinhibited, GPi and SNr send inhibitory projections to thalamus, decreasing thalamic drive to cortex and thereby inhibiting initiation of unwanted movements.

projecting to the thalamus directly, GPe neurons send GABAergic projections to the subthalamic nucleus (STN). Inhibition of the GPe by D2-SPNs in striatum results in disinhibition of the STN. When disinhibited, the STN sends excitatory projections to the GPi and SNr, reinforcing the inhibition of the thalamus and inhibiting thalamic drive of the cortex.

Dopaminergic input onto D1- and D2-SPNs originates in the substantia nigra pars compacta (SNc). Rather than acting to directly excite or inhibit striatal SPNs, dopaminergic signaling from the SNc modulates the effect of excitatory neurotransmission entering the striatum from cortex (Surmeier et al. 2007). Dopamine 1 and dopamine 2 receptors are G-protein coupled receptors (GPCRs), and agonist binding to each of these receptors results in a distinct intracellular signaling cascade. Dopamine 1 receptors are coupled to adenylyl cyclase via the alpha subunit of a GTP-binding protein, G_{olf} (Gagnon et al. 2017). Dopaminergic binding to a dopamine 1 receptor stimulates an increase in the production of the secondary messenger, cyclic adenosine monophosphate (cAMP), and increased cytosolic levels of cAMP activates protein kinase A (PKA), an enzyme that phosphorylates several downstream targets (Gagnon et al. 2017). One of the molecules phosphorylated by PKA is a dopamine- and cAMP-regulated phosphoprotein (DARPP-32). Phosphorylation of DARPP-32 converts it into a protein phosphatase-1 inhibitor, and activation of this intracellular pathway ultimately results in increased opening of L-type calcium channels, increasing the excitability of the spiny projection neuron in response to glutamatergic signaling (Beaulieu and Gainetdinov 2011).

In contrast, activation of dopamine 2 receptors negatively modulates cAMP production. Dopaminergic binding to a dopamine 2 receptor reduces cAMP levels, consequently decreasing the activation of PKA, prohibiting PKA from activating downstream targets, including DARPP-32 (Beaulieu and Gainetdinov 2011). Activation of dopamine 2 receptors inhibits L-type calcium

channels and activates G-protein coupled inwardly rectifying potassium channels, attenuating SPN excitability to glutamatergic synaptic transmission (Gagnon et al. 2017; Svenningsson et al. 2004; Beaulieu and Gainetdinov 2011).

Due to their contrasting functions in modulating striatal excitability and their distinct anatomical outputs, D1- and D2-SPNs are canonically described as playing antagonistic roles in regulating intentional movements via the direct and indirect pathways, respectively, whereby the D1-SPN "direct pathway" facilitates initiation of voluntary, desirable movements and the D2-SPN "indirect pathway" inhibits initiation of involuntary, unwanted movements. Given this framework and the symptomology of OCD, it has been suggested that OCD arises from an imbalance in the activation of direct and indirect pathways (Maia, Cooney, and Peterson 2008). Specifically, abnormal excitation of the direct pathway over the indirect pathway could conceivably give rise to the compulsive behaviors and obsessive thoughts associated with OCD.

1.1.4 Genetic basis of OCD

While the etiology of corticostriatal abnormalities in OCD are unknown, twin studies indicate a possible genetic contribution. A recent meta-analysis of twin studies reported that additive genetic effects accounted for 40% of phenotypic variance, while shared environment did not have a significant contribution (Taylor 2011). Additionally, genome-wide association studies (GWAS) indicate that genes that encode for proteins found at and around excitatory synapses may account for this genetic contribution (Kalueff et al. 2015). Specifically, disease-associated GWAS single nucleotide polymorphisms (SNPs) included *DLGAP1*, a gene that encodes a post-synaptic density scaffolding protein, and *ISM1*, a gene that is highly correlated with brain-wide expression of multiple glutamate-related genes, including members of the *DLGAP* protein family and *GRIK1*

and *GRIK4*, genes that encode for glutamate receptor subunits (Stewart et al. 2013). A second GWAS reported a significant association near the *PTPRD* gene, which encodes the receptor protein tyrosine phosphatase. PTPRD promotes the differentiation of glutamatergic synapses and interacts with SLITRK proteins which are critical for proper formation of excitatory synapses (Mattheisen et al. 2015). The relevance of this association to OCD behaviors has been investigated by knocking out *Slitrk5* in mice. *Slitrk5*-KO mice display OCD-relevant behaviors, including a self-injurious overgrooming phenotype (Shmelkov et al. 2010). Furthermore, corticostriatal neurotransmission of *Slitrk*-KOs was examined by staining for FosB in orbitofrontal cortex. FosB expression was significantly higher in *Slitrk*-KO mice relative to wild-type littermates, indicating that *Slitrk*-KO mice had higher OFC activity which is consistent with functional neuroimaging literature in OCD patients (Shmelkov et al. 2010).

1.1.5 *Sapap3*-knockout mice

While it is difficult, if not impossible, to investigate cellular and circuit mechanisms in human subjects, this can be done by utilizing animal models of compulsive behavior that display altered CSTC activity. One such model is *Sapap3*-KO mice. SAPAP family proteins are scaffolding proteins found in the postsynaptic density that act to regulate trafficking of AMPA-and NMDA-type glutamate receptors to the postsynaptic membrane of excitatory synapses (Welch et al. 2007). SAPAP3 is the only member of the SAPAP family proteins that is specifically enriched in the striatum, and mice with global deletion of the *Sapap3* gene display a compulsive grooming phenotype, often grooming to the self-injurious extent of developing skin lesions around the neck and face (Welch et al. 2007). When striatal SAPAP3 expression is rescued via lentiviral injection of SAPAP3 into the striatum specifically, the grooming phenotype of *Sapap3*-KO mice is reduced

to WT levels, providing construct validity for this animal model of striatal-dependent compulsive behavior (Welch et al. 2007). In addition to this compulsive grooming phenotype, *Sapap3*-KO mice display other OCD-relevant phenotypes including increased levels of anxiety and impaired cognitive flexibility, providing additional evidence of the relevance of this animal model for investigating the mechanisms of OCD pathophysiology (Welch et al. 2007; Manning et al. 2018).

Furthermore, corticostriatal transmission is also altered in *Sapap3*-KO mice (Welch et al. 2007; Burguiere et al. 2013). Slice physiology recordings from striatal slices of *Sapap3*-KO mice and WT littermates show that field excitatory postsynaptic potentials (fEPSPs) are significantly reduced in *Sapap3*-KOs relative to WT animals, while axonal excitability and presynaptic functions are unchanged, indicating that the change in fEPSPs is the result of postsynaptic impairments (Welch et al. 2007). Moreover, *in vivo* electrophysiological recordings of resting local field potentials in *Sapap3*-KOs and WTs show significant elevation in baseline firing rates of striatal spiny projection neurons in KOs relative to WTs (Burguiere et al. 2013). Optogenetic stimulation of lateral orbitofrontal cortex (lOFC) terminals in the central striatum results in a reduction of striatal SPN firing rates and a subsequent significant reduction of grooming levels in *Sapap3*-knockout animals (Burguiere et al. 2013). These novel findings suggest that the compulsive grooming behavior of *Sapap3*-knockout mice is causally related to alterations in CSTC circuitry, making them a relevant model to investigate how CSTC abnormalities give rise to compulsive behaviors.

Another important characteristic of *Sapap3*-knockout mice that makes them an ideal model for the present study is their treatment responsiveness. When treated with a common selective serotonin reuptake inhibitor (SSRI), fluoxetine, over the course of 6 days, grooming behavior is significantly reduced in KO mice, without affecting the grooming levels of WT littermates (Welch

et al. 2007). The underlying mechanism of this effect is currently unknown, but through exploring the effects of SSRI treatment on *Sapap3*-KO and WT cellular activity *in vivo*, researchers can glean insight into the mechanisms by which SSRI treatment is effective – or fails to be effective – in patients with OCD.

Most recently, the first post-mortem study of differential gene expression in OFC and striatum of subjects with OCD and matched comparison subjects implicated the relevance of SAPAP3 expression in OCD. Expression of the *DLGAP3* gene (synonymous with *Sapap3* in mouse genome) was significantly decreased in medial OFC, lateral OFC, nucleus accumbens core, and head of caudate in OCD subjects relative to matched comparison subjects. This finding provides further support for the hypothesis that decreases in SAPAP3 protein are involved in the generation of compulsive behaviors.

1.1.6 Selective serotonin reuptake inhibitors

SSRIs are the first-line monopharmacotherapy for OCD. While other psychotropic medications, including mood stabilizers, tricyclic antidepressants, benzodiazepines, and monoamine oxidase inhibitors all fail to have any effect on the core symptoms of OCD, SSRI treatment yields symptom improvement in 40-60% of patients (Goddard et al. 2008). However, nearly half of patients report feeling no significant change in their symptoms with SSRI treatment, and full remission is achieved with this pharmacologic treatment in only 25% of the patient population (Goddard et al. 2008).

SSRIs act by blocking the serotonin transporter (5-HTT) to increase intrasynaptic concentrations of serotonin. Importantly, in addition to increasing levels of serotonin in the frontal cortex, striatum, and hippocampus, acute SSRI administration also serves to decrease the

functional connectivity between cortical and subcortical regions(van de Ven et al. 2013; McCabe et al. 2011). Given that cortical-subcortical connectivity is significantly increased in untreated OCD patients relative to healthy controls (Harrison et al. 2009), SSRI treatment may serve to attenuate symptoms by normalizing activity throughout the corticostriatal circuit.

The mixed effectiveness of SSRIs for managing OCD symptoms is reflective of the fact that this pharmacologic treatment is unspecific, and the mechanism by which SSRIs decrease obsessional and compulsive symptoms is largely unknown. Chronic SSRI administration alters serotonergic neurotransmission, often depleting concentrations of tryptophan (a precursor to serotonin) and serotonin (Goddard et al. 2008). In major depressive disorder, symptom management with SSRIs depends on maintaining the availability of presynaptic serotonin, but in OCD, the therapeutic effect of SSRI administration appears to be unaltered by serotonin depletion, indicating that the mechanism of action by which SSRIs attenuate OCD symptoms is long-term and based in changes at the post-synaptic density (Goddard et al. 2008; Berney 2005; Barr LC 1994). While it is encouraging that SSRIs provide symptomatic relief to a subset of OCD patients, it is important to investigate the underlying mechanism by which SSRIs grant symptomatic relief, such that this mechanism can be exploited and improved upon to yield greater therapeutic efficacy as a pharmacotherapy for OCD.

1.1.7 *In vivo* calcium imaging

In vivo calcium imaging enables researchers to record cellular activity from hundreds of neurons per mouse while maintaining spatial information, a large advance from traditional electrophysiological techniques (Resendez et al. 2016). After acquiring spatial information from each neuron that is active in each recording session, researchers are able to track the activity of

individual neurons over the course of multiple sessions and to assess how changes in the experiment such as the administration of a specific drug affects the activity of individual cells, giving rise to the global, nonspecific changes that traditional electrophysiological techniques detect. Furthermore, this method allows researchers to record activity from genetically-distinct cell populations, as opposed to recording from all neurons within a given region (Resendez et al. 2016).

When relying on model systems of psychiatric disease states, it is of significant importance that the experimental methods do not inhibit animals from performing normal behaviors. In this particular model system, the behavior of interest is compulsive grooming, so it is necessary that mice are able to carry out this behavior without being constrained due to the experimental method being utilized. While *in vivo* electrophysiology rigs confer an excess of weight that makes it difficult for mice to perform this behavior and *in vivo* two-photon fiber photometry requires animals to remain in a head-fixed position, *in vivo* calcium imaging enables mice to move about the behavioral chamber freely with head-mounted microscopes that are sufficiently light-weight not to significantly alter behavior (Resendez et al. 2016).

More specifically, *in vivo* calcium imaging is achieved by injecting an adeno-associated virus (AAV) expressing GCaMP6m, a genetically encoded calcium indicator. GCaMP6m is comprised of green fluorescent protein (GFP), the calcium-binding protein calmodulin, and calmodulin-interacting peptide 13 (Chen et al. 2013). When the intracellular calcium concentration of a neuron is significantly increased (when a neuron fires an action potential), GCaMP6m undergoes a conformational change that results in the GFP chromophore fluorescing (Chen et al. 2013). Therefore, observing bursts of calcium fluorescence can be used as a reliable and representative proxy for neural activation that can be observed *in vivo* at single-cell resolution.

1.2 Specific aims of current work

This thesis investigates the neural activity patterns of compulsive behavior in a mouse model of OCD-relevant behavior. Using novel *in vivo* calcium imaging technology, I will assess calcium activity in the central striatum of *Sapap3*-KO mice and WT littermates to determine if there are genotype differences in grooming-associated calcium activity. Additionally, I will investigate the effects of SSRI treatment on compulsive grooming behavior and calcium activity in the central striatum. In Experiment 1, I examine the combined activity of D1- and D2-SPNs by utilizing a synapsin promoter GCaMP6m lentivirus. In Experiment 2, I begin to investigate the roles of individual SPN subpopulations in the manifestation of compulsive behaviors. Here, I examined the grooming-associated activity of D1-SPNs by injecting a Cre-dependent GCaMP6m virus into central striatum of D1-cre x *Sapap3*-KO and D1-cre x *Sapap3*-WT mice. Thus, this work will contribute to the present understanding of the role of central striatum in compulsive behaviors and shed light on the neural mechanisms by which effective SSRI treatment reduces behavioral compulsivity.

2.0 METHODS

2.1 Experiment 1 (Synapsin Cohort)

2.1.1 Subjects

All procedures were conducted in accordance with the National Institute of Health's *Guide to the Care and Use of Laboratory Animals* and approved by the University of Pittsburgh's Institutional Animal Care and Use Committee**.** *Sapap3*-knockout (*Sapap3*-KO) and wildtype (WT) littermates on 100% C57BL/6 background were bred using *Sapap3* heterozygous mutants ($Sapap3^{+/-}$). For Experiment 1, five adult male *Sapap3*-KO mice and five adult male WT mice were utilized, and behavioral and neuronal data were collected from all animals. Each animal was housed on a 12-hour light cycle (lights on at 7AM), and all mice were approximately 4-6 months old at the time of the first surgical procedure.

2.1.2 Stereotactic surgery

In the first surgical procedure, mice were anesthetized using 5% isoflurane mixed with oxygen and maintained on 1-2% isoflurane throughout the duration of the surgery. Mice were placed on a small-animal stereotactic instrument (Kopf Instruments) and secured using a bite bar and ear bars. Hair was removed from the dorsal surface of the head with hair clippers, and the surface of the head was scrubbed with a betadine solution. After sterilizing the dorsal surface of the head, a large incision was made such that the dorsal portion of the skull was exposed. Skull surface was cleared

of remaining musculature and tissue, and bregma was located. All surgical measurements were made relative to the interpolated bregma. First, two .45mm skull screws were placed anterior to the lambdoid suture for stability. Then, a large skull window was made in the surrounding area of viral and implant targeting (AP: +.65mm, ML: -1.8mm), and the surgical cannula was zeroed to dura. Dura was removed prior to lowering surgical cannula into the brain.

Viral injections were performed using a fixed needle Hamilton syringe (Cole-Parmer Scientific, Vernon Hills IL, USA) connected to sterile polyethylene tubing affixed to a metal cannula and a Harvard Apparatus Pump 11 Elite Syringe Pump (Harvard Apparatus, Holliston MA, USA). 800 nl of a virus encoding GCaMP6m under the synapsin promotor (AAV9-synapsin-GCaMP6m-WPRE-SV40, 2.3e13**)** were injected into the central striatum (AP: +0.65mm, ML: -1.8mm, DV: -2.9mm & -3.0mm). Injections were performed in a series of two steps, with 400nl of virus injected at DV = -2.9mm and 400nl of virus injected at DV = -3.0mm. Immediately following viral injection, a 500-µm-diameter graded-index lens (ProView GRIN lens, Inscopix Pala Alto, CA USA) was lowered just dorsal to the viral injection target (AP: +0.65mm, ML: -1.8mm, DV: -2.85mm) to allow for visualization of cells in the target region.

Following lens lowering, acrylic dental cement (Lang Dental, Wheeling IL, USA) was utilized to create a temporary head cap that secured lens placement and sealed off the GRIN lens during the incubation period (4-6 weeks). Following completion of surgery, mice were injected with sub cutaneous (s.c.) carprofen, and topical antibiotic ointment (TAO) and lidocaine were administered around the temporary head cap. Mice were then placed on a heating pad, given DietGel, and monitored until they fully recovered from anesthesia. Mice were administered carprofen s.c. and received lidocaine and TAO treatments for 3 days post-surgery. For all surgical

procedures, mice were group-housed with littermates unless conspecific fighting was noted. In such cases, the aggressive mouse was isolated for the duration of the experiment.

After waiting 4-6 weeks to allow for sufficient viral incubation, animals were anesthetized with 5% isoflurane and secured to a stereotactic apparatus using ear cuffs and a bite bar. Mice were maintained on 1-1.5% isoflurane for the duration of the second surgical procedure. First, the temporary head cap fashioned from acrylic dental cement was carefully removed using a Dremel tool until the ProView GRIN lens was exposed. The top of the ProView lens was then cleaned with compressed air and lens paper to remove all dental cement dust. A magnetic microscope baseplate (Part ID:1050-002192, Inscopix) was then attached to the miniaturized microscope (nVistaHD 2.0 epifluorescence microscope, Inscopix) and lowered into place above the GRIN lens with the 475nm blue LED gain and power of the miniaturized microscope set to their maximum levels. Because cellular activity is minimal in deep structures such as the striatum when animals are anesthetized, vasculature was used as a main landmark that enabled proper focusing and alignment of the miniaturized microscope. Once an optimal field of view was obtained, the baseplate was secured in place using dental cement, and a plastic Microscope Baseplate Cover (Part ID:1050-002193; Inscopix) was attached to prevent debris from blocking the lens.

2.1.3 Drug preparation and administration

(±)Fluoxetine hydrochloride (Fluoxetine) was obtained through the NIMH Chemical Synthesis and Drug Supply Program. Fluoxetine was administered intraperitoneally (i.p.) according to previous studies which report a reduction in *Sapap3*-KO grooming following treatment (Welch et al. 2007). *Sapap3*-KO and WT mice received 5mg/kg fluoxetine in a .9% saline solution

(10mL/kg) injected i.p. daily for 7 consecutive days, consistent with the protocols outlined by (Welch et al. 2007).

2.1.4 Grooming behavior and *in vivo* calcium imaging

Each mouse was given a minimum of 7 days to recover from surgery before being habituated to the experimental chamber and miniaturized microscopes. In order to attach the microscope securely to the baseplate, mice were lightly scruffed while the miniature nVistaHD 2.0 microscope was connected to the magnetic baseplate and secured with a set screw. Mice were then placed in a clear acrylic chamber (8" W x 8" D x 12" H) for 5-10 minutes once daily on three consecutive days. During behavioral habituation, the gain and power of the miniaturized microscope LED were adjusted to optimize visualization of calcium fluorescence. Microscope focus was also adjusted and recorded using a caliper tool to assist in consistent placement of the microscope throughout consecutive days of the experiment.

Following three days of habituation, baseline grooming behavior was assessed. To accurately capture behavioral activity, a behavioral acquisition camera (Point Grey Blackfly, FLIR Integrated Imaging Solutions) was placed below the behavioral chamber, recording from a bottom-up perspective. Behavioral acquisition was conducted at 40 Hz using SpinView (Point Grey) software, and detailed frame information was sent directly to a central data acquisition box (LabJack U3-LV, Labjack Corporation, Lakewood CO USA). A randomly flashing (30s ITI) LED was visible in the field of view of the behavioral acquisition camera throughout the entire testing session. This LED was controlled by custom scripts via an Arduino (Arduino Leonardo, Somerville MA, USA) and sent TTL pulses to the LabJack, enabling accurate alignment of behavior and calcium data.

On the baseline day of Experiment 1, grooming behavior was recorded for forty-minutes, and *in vivo* calcium activity in the striatum was simultaneously recorded throughout the entire session. After the microscope was attached, mice were left in a cage without cage mates for 3-5 minutes, allowing time for animals to recover from scruffing and for any rapid photobleaching of calcium signal to occur. Mice were then carefully placed in the clear acrylic chamber. LabJack data acquisition was started, immediately followed by behavioral SpinView recordings from behavioral acquisition camera and nVistaHD software recording of compressed greyscale tiff images at 20Hz. Individual calcium frame information was sent to the LabJack as it simultaneously received behavioral frame acquisition, enabling subsequent alignment of behavior and calcium data. For all mice, analog gain of the image sensor was set between 1 and 4 while the 470 nm LED power was set between 10 to 30% transmission range. These settings were kept consistent for each mouse throughout all subsequent imaging sessions.

Following the baseline day of Experiment 1, animals received one week of fluoxetine treatment. 5mg/kg fluoxetine hydrochloride in a .9% saline solution (10mL/kg) was injected i.p. daily for 7 days**.** On the eighth day, grooming behavior and calcium activity were reassessed in another forty-minute session following the same protocol used on the baseline day. After fluoxetine treatment had been completed for two weeks, a final assessment of grooming behavior and calcium activity was recorded for a forty-minute session. Again, this session adhered to the same protocol used on the baseline day and treatment day 7.

2.1.5 Behavioral analysis

Following acquisition of behavioral data, video files were converted and compressed (maintaining accurate frame rate information) into .MP4 format using the open source software HandBrake.

Videos were imported into Noldus The Observer XT (Noldus Leesburg VA, USA). Animal grooming behavior was scored frame-by-frame by observers that were blind to experimental conditions. Three grooming behaviors were assessed: facial grooming, body grooming, and hind-leg scratching (Figure 2.1) The start of a facial grooming bout was defined by the frame in which the animal started to move its front limbs from the ground toward the face. The start of a body grooming bout was defined by the frame in which the animal shifted its weight and began to turn its head toward its flank. The start of a hind-leg scratching bout was defined by the frame in which the animal positioned its weight and started to lift a hind-leg toward its flank or face. The cessation of all grooming bouts was defined by the frame in which the animal had fully completed the grooming behavior and returned to a neutral body position.

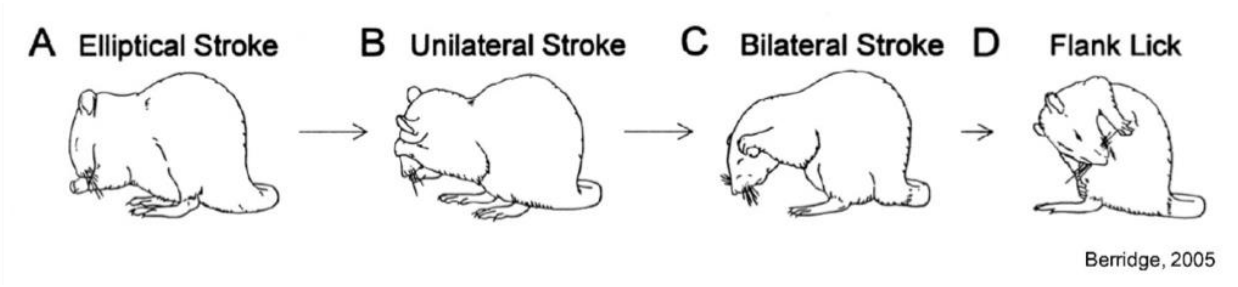

Figure 2.1 Pictorial Example of Grooming Behaviors

This figure shows representative examples of grooming behaviors. (A), (B), and (C) represent facial grooming in which the mice grooms around its snout, face, and ears. (D) represents body grooming in which the animal turns to one side to lick their flank. This figure was adapted from (Berridge et al. 2005).

2.1.6 Calcium imaging data processing

All imaging pre-processing was performed using Mosaic software **(**Mosaic 1.2.0**,** Inscopix) via custom Matlab (MATHWORKS, Natick MA, USA) scripts. Videos were spatially downsampled by a binning factor of 4 (16x spatial downsample) and temporally downsampled by a binning

factor of 2 (down to 10 frames per second). Lateral brain motion was corrected using the registration engine TurboReg (Ghosh et al. 2011) which uses a single reference frame to match the XY positions of each frame throughout the video. Motion-corrected 10 Hz video of raw calcium activity was then saved as a .TIFF and used for cell identification.

Using custom Matlab scripts, the motion-corrected .TIFF video was processed using the Constrained Non-negative Matrix Factorization approach (CNMFe), which has been optimized to isolate signals from individual putative neurons from microendoscopic imaging (Zhou et al. 2018). The CNMFe method is able to simultaneously denoise, deconvolve, and demix imaging data (Pnevmatikakis et al. 2016) and represents an improvement over previously used algorithms based on principle component analysis (Zhou et al. 2018). The primary improvement comes from accurate estimation and subtraction of both local and global background fluorescence signal, providing better separation of densely packed cells and a cleaner overall calcium signal from individual putative cells.

After processing in CNMFe, putative neurons were identified and manually sorted by an observer blind to genotype according to previously established criteria (Resendez et al. 2016). For the data presented in this thesis, I report the non-denoised temporal traces (referred to as the "raw" trace in CNMFe) without any deconvolution. For each individual cell, the raw fluorescence trace was Z-scored to the average fluorescence of that same trace. Thus, fluorescence units presented are referred to as "Z-scored fluorescence".

2.1.7 Calcium imaging analysis

Custom Matlab (MATHWORKS) scripts were used to analyze of grooming-associated calcium activity. Grooming behaviors (state events) were exported as timestamps (grooming start and

grooming stop) and aligned to calcium time based on the first 5 consecutive LED pulses recorded from the behavioral acquisition camera (point events). The offset of Noldus behavior time to nVista calcium time was then subtracted off, leaving the same number of frames for both the behavior and calcium fluorescence. Grooming timestamps were transferred to a binary/continuous trace of the same length and sampling rate (10 Hz) as each calcium trace via logical indexing (grooming = 1, not-grooming = 0). Timestamps for behavior were converted to the closest matching frame in the calcium recording (maximum error of ± 100ms at 10 Hz). Calcium activity could then be aligned to the start and end of a grooming bout, or to the transition point between one grooming bout and another (when there was ≤ 1s between a grooming bout ending and a grooming bout beginning).

2.1.7.1 Unbiased event-related activity classification

A more precise method of analyzing calcium imaging data is assessing if the calcium activity of each individual cell is modulated by a behavioral event of interest (in this case, grooming). In this study, cells were categorized as activated by grooming-onset, inhibited by grooming-onset, or unaffected by grooming-onset. To quantitatively classify the grooming onset-responsiveness of each cell, we adapted a strategy used in (Jimenez et al. 2018) using custom Matlab (MATHWORKS) scripts. For each cell, we first aligned raw calcium fluorescence to the onset of each grooming bout. These traces were then averaged across all bouts within a given testing session. For each cell, we assessed raw calcium fluorescence for 10s prior to and 10s following grooming onset. Each instance of grooming-onset is defined as an individual trial, and trials are subdivided into 200 individual time bins at 10Hz (100ms per sample). Individual time bins were shuffled in time for each trial (200x) to remove any temporal information that was previously in each trace while maintaining the variance within each grooming bout. This shuffle was repeated

1000 times per cell to obtain a null distribution of grooming-associated calcium activity. A cell was classified as responsive to grooming onset if its Z-normalized calcium fluorescence amplitude between -0.5s before grooming onset to 3s after grooming onset exceeded ± 1 standard deviation threshold from the null distribution. If the average calcium signal of a cell exceeded +1 standard deviation of the shuffled average calcium signal, the cell was categorized as activated. If the average calcium signal of a cell exceeded -1 standard deviation of the shuffled average calcium signal, the cell was categorized as inhibited. Cells with calcium signal that fell within ± 1 standard deviation of the shuffled average calcium signal were determined to be unaffected by grooming onset (activity is not significantly modulating by grooming-onset). Individual cells classified as activated or inhibited by grooming onset could then be averaged across genotype and directly compared within and across sessions, providing an assessment of how cells encoding grooming differ across genotype or with drug treatment.

2.1.7.2 Accurate cell matching across sessions

Putative neurons were matched using a probabilistic modeling method detailed in (Sheintuch et al. 2017). The cell matching occurred across two sessions and was performed using the following steps. First, centroid location for all cells were projected onto a single image. Slight rotation and translation difference between sessions were adjusted to achieve maximal cross-correlation between sessions. Probabilistic modeling was then employed to determine which model (centroid distance vs spatial correlation) was optimal for each set of data. For all data, the spatial correlation model yielded the best results and was thus used to match cells across sessions. For final alignment, the spatial correlation (not the joint model) was used, and correlation values for nearest neighbors was set at ≥ 0.70.

2.1.8 Statistical analysis

Statistical analysis was carried out using custom Matlab scripts (MATHWORKS) or GraphPad Prism 8.0 (GraphPad Software, San Diego CA, USA). Throughout this thesis, results are reported as mean ± SEM unless otherwise noted.

2.1.8.1 Statistical analysis of grooming behavior

Baseline grooming behavior in *Sapap3*-KOs and WTs was analyzed using two-tailed independent samples *t*-tests. To analyze behavioral changes following fluoxetine administration, a two-way repeated measure analysis of variance (ANOVA) was used. Main effects and interaction terms are reported throughout, and in cases of significant interactions, post-hoc comparisons were made using Sidak's multiple comparison correction. A corrected alpha was set to 0.05.

2.1.8.2 Statistical analysis of calcium imaging data

In order to evaluate the effect of genotype and treatment on grooming-evoked calcium fluorescence averaged across individual cells, unpaired two-tailed *t*-tests were performed at each time bin (100ms). Due to our high *N* with dozens to hundreds of cells in each condition, a conservative Bonferroni correction was performed at $\alpha = \frac{0.05}{m}$. The critical *p* value ($\alpha = 0.05$) was divided by the total number of time bins (each bin = 100ms) to be compared (m), resulting in adjusted critical values between 0.00025 and 0.0005, depending on the exact comparison.

For comparison of proportions of classified cells during baseline imaging sessions, two-tailed independent samples *t*-tests were used. To assess the effect of fluoxetine treatment on the proportions of classified cells, two-way repeated measures ANOVA were used. When a significant

interaction between genotype and drug treatment was observed, post-hoc tests were conducted using Sidak's multiple comparisons test. A corrected alpha was set to 0.05.

2.1.9 Histology

Following the completion of all experiments, animals were perfused with phosphate buffered saline (1X PBS) followed by 4% paraformaldehyde (PFA). Brains were extracted and post-fixed in 4% FPA for 24 hours. They were then transferred to a 30% sucrose azide solution for 24-48 hours. Brains were sliced at -20ºC into 35µm slices using a Leica CM3050 cryostat**,** and slices were stored in wells containing a 1X PBS + .1% NaN_3 solution. Slices were mounted onto slides from 1X PBS, cover-slipped with Fluoroshield™ with DAPI mounting medium and visualized using a scanning microscope at 10x magnification to confirm viral expression and proper lens placement in mouse central striatum as specified by Paxinos and Franklin's *The Mouse Brain in Stereotactic Coordinates: 4th Edition*.

2.2 Experiment 2 (D1-cre Cohort)

2.2.1 Subjects

All procedures were conducted in accordance with the National Institute of Health's *Guide to the Care and Use of Laboratory Animals* and approved by the University of Pittsburgh's Institutional Animal Care and Use Committee. For Experiment 2, D1-cre positive x *Sapap3*-KO and D1-cre *Sapap3*-WT mice on 100% C57BL/6 background were generated by breeding D1-cre positive mice with heterozygous mutants (*Sapap3*$^{+/-}$). Six adult (four male, two female) D1-cre x *Sapap3*-KO mice and eight adult (three male, five female) D1-cre x *Sapap3*-WT mice were utilized in this experiment, and behavioral and neuronal data were collected from all animals. Each animal was housed on a 12-hour light cycle (lights on at 7AM), and mice were approximately 4-6 months old at the time of the first surgical procedure.

Surgical procedures were identical to those described for Experiment 1 in Section 2.1.2 with the exception of viral strain. For this experiment, mice were injected with 800nl of Cre-dependent GCaMP6m (AAV9-Syn-Flex-GCaMP6m-WPRE-SV40, 2.7e13) into the central striatum (AP: +0.65mm, ML: -1.8mm, DV: -2.9 & -3.0mm). Injection of this D1-promoter virus allowed *in vivo* visualization of D1-SPNs. All behavioral protocols, drug treatment protocols, and behavioral and calcium imaging analysis performed in Experiment 2 were the same as in Experiment 1 (see Section 2.1 above for details).

3.0 RESULTS

3.1 Experiment 1 Results (Synapsin Cohort)

3.1.1 *Sapap3*-knockouts groom more than wild-types with microscope attached

Previously it has been reported that *Sapap3*-knockout (KO) mice spend significantly more time grooming than wild-type (WT) littermates (Welch et al. 2007). Consistent with previous findings, we observed that the compulsive grooming phenotype of *Sapap3*-KOs is maintained following surgical implantation of a microendoscope and attachment of a 2-gram miniature microscope. Relative to WT littermates, *Sapap3*-KOs spent a significantly longer time engaged in grooming throughout a 40-minute testing session (Fig. 3.1A; $t(8) = 4.84$, $p = .001$), and *Sapap3*-KOs performed more individual grooming bouts than WT counterparts (Fig. 3.1B; $t(8) = 2.81$, $p = .023$).

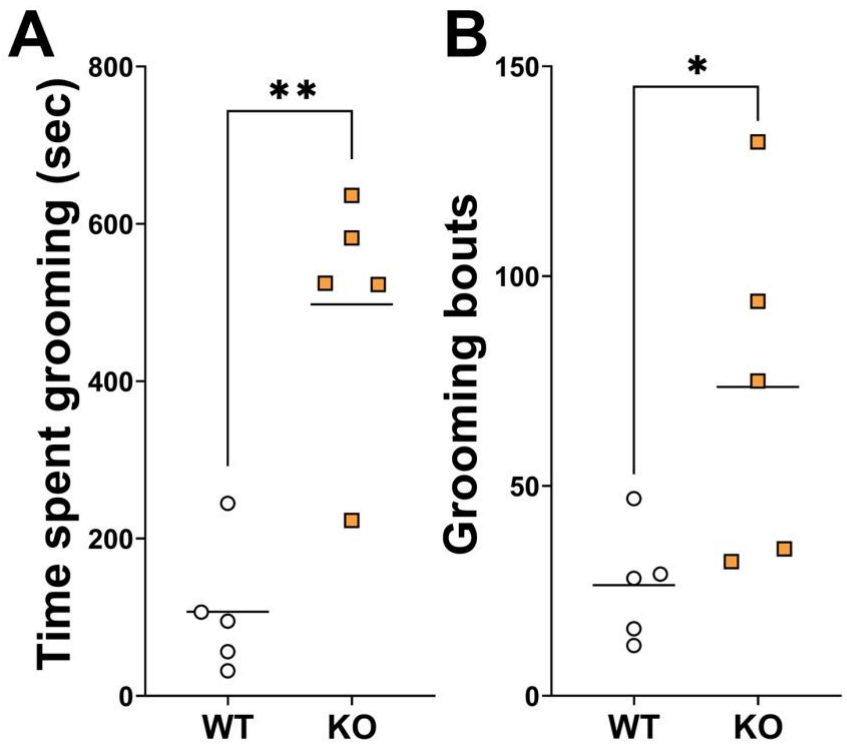

Figure 3.1 Total Grooming Time and Number of Grooming Bouts

(A) *Sapap3*-KO mice spent significantly more time grooming during 40-minute testing session relative to WT mice. (B) *Sapap3*-KO mice initiated a significantly higher number of grooming bouts throughout the course of the session relative to WT mice. (**$p < .01$, *$p < .05$)

3.1.2 Central striatum of *Sapap3*-KO mice is hyperactive during compulsive grooming

After aligning behavioral activity with striatal calcium activity, we examined each individual cell's response to the beginning of grooming behavior and averaged the response of each cell to all instances of grooming-onset that occurred throughout the 40-minute testing session to obtain Z-normalized fluorescence of each cell at grooming onset. With an average of over 100 cells detected per animal, we then compiled each cell's normalized calcium fluorescence at grooming onset in each group (WT and KO).

Cells were sorted based on normalized fluorescence at grooming onset (t = 0), from greatest to least fluorescence. We displayed each cell's normalized calcium fluorescence for a 10s-time frame surrounding grooming onset (5s prior to groom-start through 5s after groom-start), generating heat plots of normalized calcium fluorescence at grooming-onset within each group (Figure 3.2). In examining the respective heat plots for grooming-onset in the striatal cells of KOs and WTs, it is apparent that more cells from KO mice exhibit higher normalized calcium fluorescence at the onset of grooming, and this increased fluorescence appears to persist following grooming-onset.

Next, we averaged normalized fluorescence of all cells within each group at each individual 100ms time bin from 5s prior to through 5s following grooming-onset. These collapsed traces were compared across genotype using t-tests and corrected for multiple comparisons. In doing so, we found that normalized calcium fluorescence was significantly increased in the SPNs of KO mice relative to WT mice beginning at approximately 1s prior to grooming onset and persisting for 5s following grooming onset. (Figure 3.3; All significant values had $t(733) \geq 4.086$ and $p \leq .000049$.)

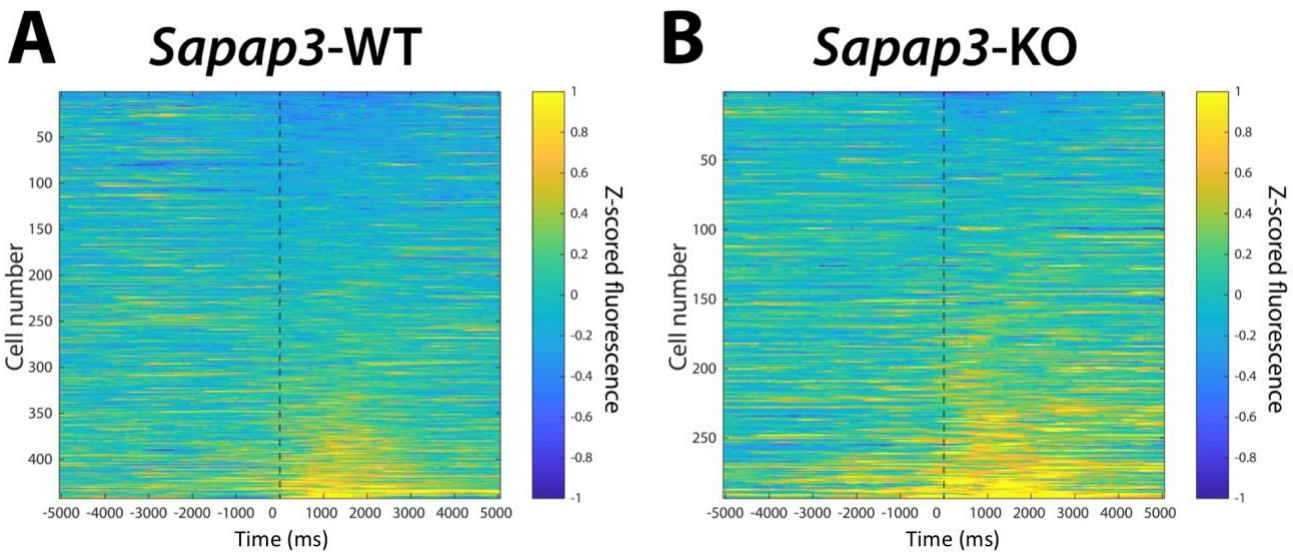

Figure 3.2 Heatplots of Normalized Calcium Fluorescence of Individual Cells to Grooming Onset

Normalized calcium fluorescence is plotted as a function of color and aligned to the onset of grooming behavior in *Sapap3*-KOs (Figure 3.2A) and WTs (Figure 3.2B). Data are depicted as the average fluorescence response evoked at the onset of grooming bouts, and neurons were sorted based on calcium fluorescence at time = 0ms (the instant a grooming behavior is initiated). Normalized fluorescence appears to be increased at and following grooming-onset in *Sapap3*-KOs, an effect not observed in WT mice.

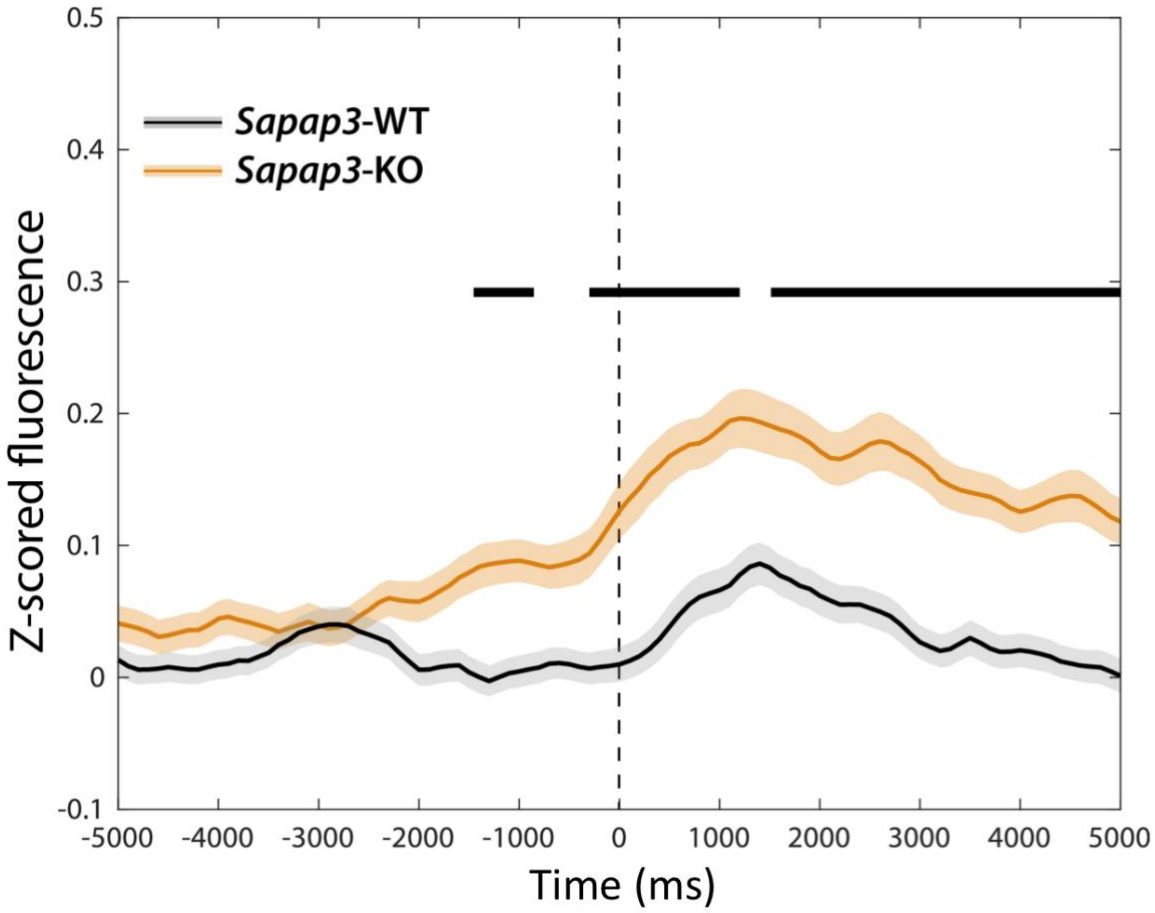

Figure 3.3 Averaged Calcium Fluorescence Across All Cells at Grooming Onset

This figure shows the normalized fluorescence of all cells collapsed to generate composite traces for each *Sapap3*-KOs and WTs. SPNs of *Sapap3*-KOs show a large transient increase in fluorescence in response to grooming onset that persists for several thousand milliseconds, and this effect is not observed in SPNs of WT mice. This suggests that the central striatum of *Sapap3*-KOs is hyperactive at grooming onset (bar indicates all $t(733) \geq 4.086$, $p \leq .000049$).

3.1.3 No significant difference in amplitude of grooming-modulated spiny projection neurons of *Sapap3*-KO and WTs

Several underlying factors could contribute to our observation of increased calcium fluorescence at grooming onset in KOs relative to WT mice. One possibility is KOs and WTs may have equal numbers of groom onset-activated SPNs, but the amplitude of groom onset-activated SPNs in KOs is greater than the amplitude of groom onset-activated SPNs in WTs. This difference would be shown by greater normalized fluorescence at grooming onset in groom onset-activated SPNs of KOs relative to WTs. Conversely, this effect could be observed if the amplitude of cells that are inhibited at grooming onset in KO mice significantly differs from that of WT mice. Specifically, if groom onset-inhibited SPNs in WT mice were inhibited to a stronger degree that groom onset-inhibited SPNs of KOs, then normalized fluorescence at grooming onset in groom onset-inhibited SPNs of KOs would be elevated relative to normalized fluorescence at grooming onset in groom onset-inhibited SPNs of WT mice.

To investigate these possibilities, we assessed if the amplitude of activity-modulated SPNs differed across genotype. We first categorized all SPNs in each group as activated, inhibited or unaffected by groom-onset using the strategy described in Section 2.1.7.1. After separating out all activated units in KOs and WTs, we averaged across all activated units within each genotype. We also separated out all inhibited units in KOs and WTs and averaged across all inhibited units within each genotype. When comparing the average amplitude of activated and inhibited units of KOs and WTs, we did not find any significant differences for either activated or inhibited SPNs across genotype. Within activated cells, the amplitude difference that was closest to significance was $t(123) = 2.78$, $p = .0062$ (Figure 3.4A). Within inhibited cells, the amplitude difference that was closest to significance was $t(41) = 2.5693$, $p = .0139$ (Figure 3.4B).

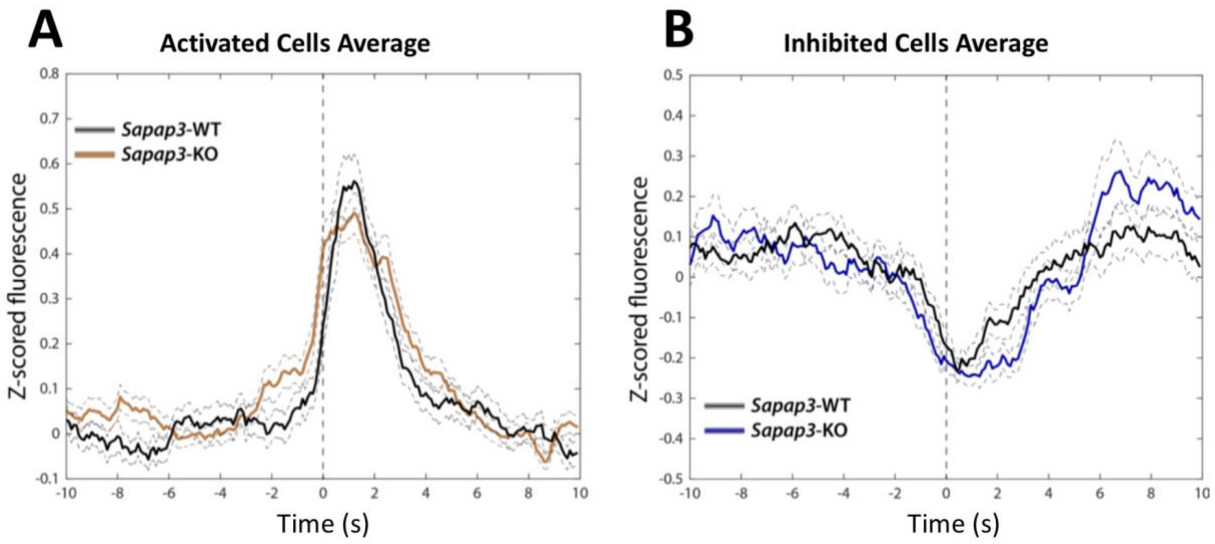

Figure 3.4 No Difference in Amplitude of Grooming-Modulated Spiny Projection Neurons

This figure shows the normalized calcium fluorescence of all cells that are modulated by grooming-onset in *Sapap3*-KO and WT mice. (A) There is no significant difference in amplitude of groom onset-activated cells across genotype (all $t(123) \leq 2.78$, all $p \geq .0062$). (B) There is no significant difference in amplitude of groom onset-inhibited cells across genotype (all $t(41) \leq 2.57$, all $p \geq .0139$). Dashed gray lines represent error bars, showing the range of Z-scored fluorescence elicited from groom onset-modulated SPNs.

3.1.4 *Sapap3*-KOs have more grooming onset-activated spiny projection neurons than WTs

Given that we did not discover a difference in amplitude of grooming-modulated SPNs in *Sapap3*-KOs relative to WTs, we hypothesized that the increased calcium fluorescence at grooming onset observed in KO mice was driven by a difference in the percentage of total SPNs that are positively or negatively modulated by grooming onset. Specifically, this difference could be the result of an increased percentage of groom onset-activated SPNs in *Sapap3*-KO mice relative to WT mice or a decreased percentage of groom onset-inhibited SPNs in *Sapap3*-KO mice relative to WT mice. Using the cell sorting methods described in Section 2.1.7.1, we assessed the activity-modulation of all SPNs in *Sapap3*-KOs and WTs. We found that a significantly higher percent of total SPNs were activated by grooming onset in *Sapap3*-KO mice relative to WT mice (Figure 3.5B; $t(8) = 4.846$, $p = .0013$). There was no significant difference in the percentage of cells inhibited by grooming onset across genotype (Figure 3.5B; $t(8) = .672$, $p = .5205$). This finding indicates that the overall striatal hyperactivity that is observed in *Sapap3*-KOs at grooming onset may be due to the recruitment of a greater number of striatal SPNs at the initiation of a grooming behavior.

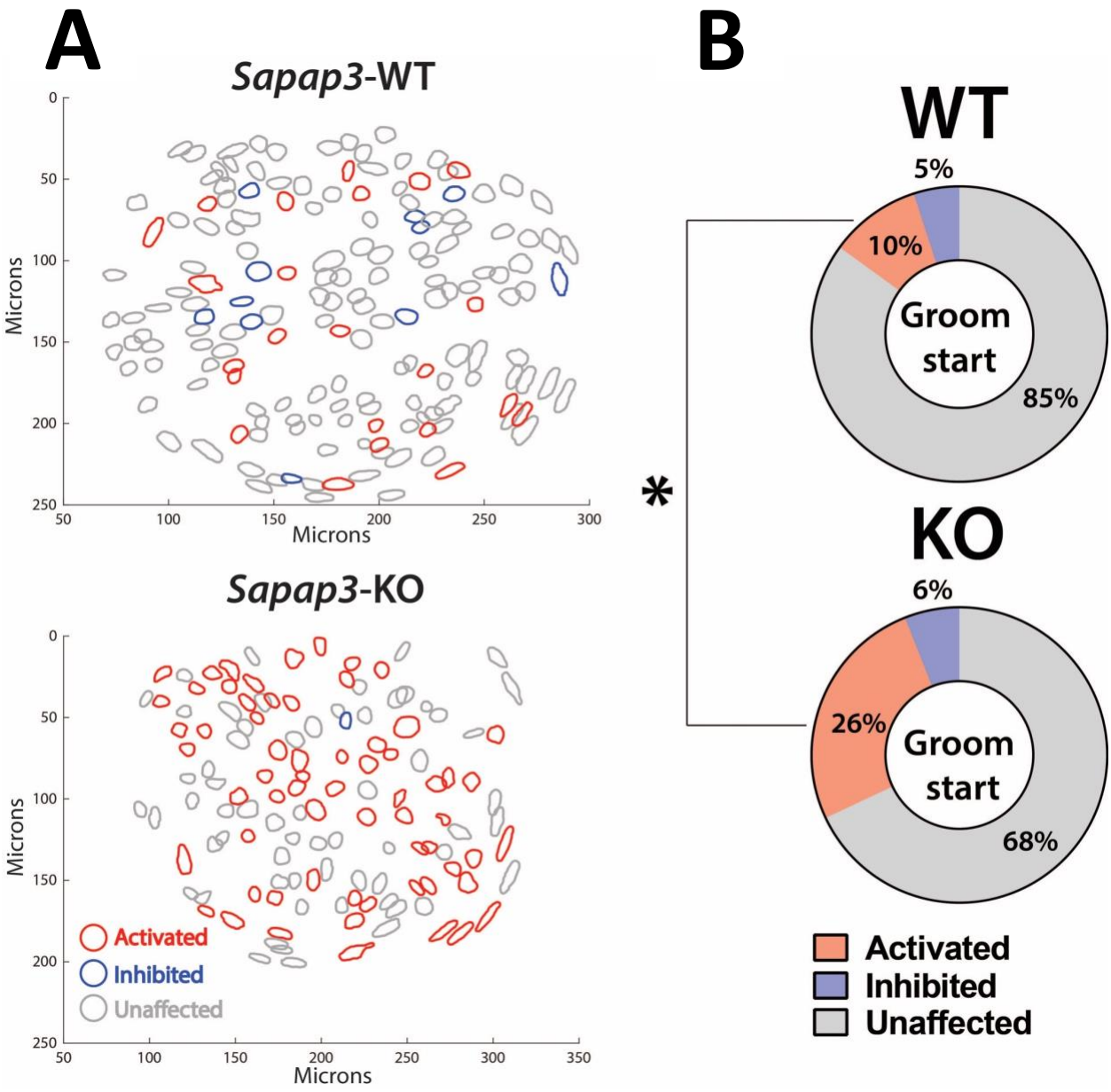

Figure 3.5 Grooming-Modulated Cell Populations

(A) A representative sample of SPNs from one WT and one KO mouse that were identified as activated, inhibited, or unaffected by grooming onset. (B) A significantly higher percentage of groom onset-activated cells were observed in *Sapap3*-KOs relative to WT mice. There was no significant difference in the percentage of groom onset-inhibited SPNs across genotype. (*$p < .05$)

3.1.5 Fluoxetine reduces compulsive grooming in *Sapap3*-KO mice

Previous studies report that the compulsive grooming phenotype of *Sapap3*-KO mice can be reversed by acute SSRI treatment (Welch et al. 2007). Here, we treated *Sapap3*-KO and WT mice with 5mg/kg FLX in a .9% saline solution (10mL/kg) injected i.p. daily for 7 consecutive days. We found that there was a main effect of genotype on time spent grooming ($F(1,8) = 12.55$, $p = .0076$) as well as a main effect of FLX treatment ($F(1,8) = 13.71$, $p = .0060$). Additionally, there was an interaction between genotype and FLX treatment ($F(1,8) = 17.59$, $p = .0030$). Post hoc comparisons showed that 7 days fluoxetine treatment significantly reduced time spent grooming in *Sapap3*-KO mice **(**Figure 3.6A; $t(8) = 5.584$, $p = .0010$) but not in WT mice (Figure 3.6A; $t(8) = .3476$, $p = .9309$). We also found a main effect of genotype on grooming bout number ($F(1,8) = 3.941$, $p = .0824$) as well as a main effect of FLX treatment ($F(1,8) = 3.465$, $p = .0997$) and an interaction between genotype and FLX treatment ($F(1,8) = 3.465$, $p = .0997$). Post hoc comparisons showed that 7 days of fluoxetine significantly reduced number of grooming bouts initiated by *Sapap3*-KO mice (Figure 3.6B; $t(8) = 2.633$, $p = .0592$) but not WT mice (Figure 3.6B; $t(8) = 0.0$, $p = 1.0$).

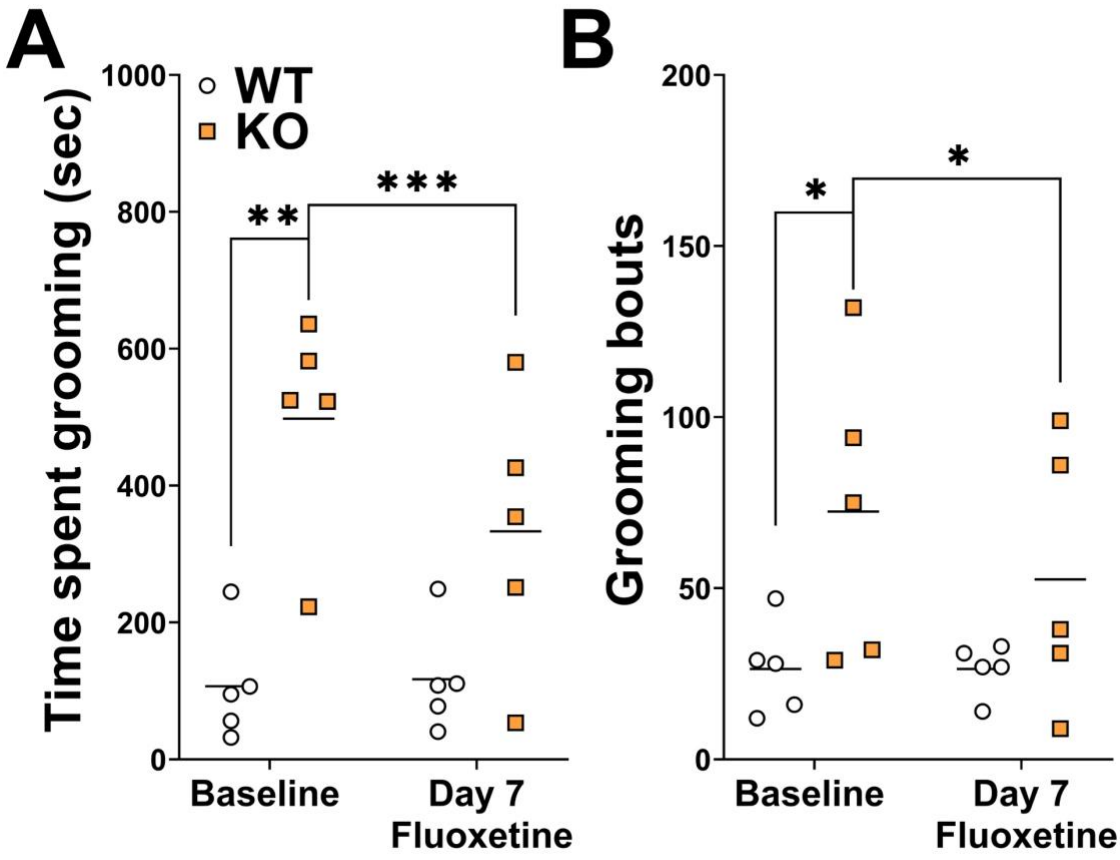

Figure 3.6 Grooming Time and Bout Number at Baseline and Following 7 Days Fluoxetine Treatment

(A) At baseline, *Sapap3*-KO mice spent a significantly longer time grooming in a 40-minute session relative to WT mice and initiated significantly more individual grooming bouts. Following 7 days of fluoxetine administration, grooming was significantly reduced in KO mice, but grooming levels of WT mice were unaffected. (B) At baseline, *Sapap3*-KO mice engaged in a significantly higher number of grooming bouts. After 7 days of fluoxetine administration, *Sapap3*-KO mice had a significant reduction in grooming bout number. These findings indicate that fluoxetine is capable of reducing compulsive grooming in *Sapap3*-KO mice and that drug administration does not affect activity of WT animals. (***$p < .001$, **$p < .01$)

3.1.6 Fluoxetine reduces percentage of cells activated at grooming-onset in *Sapap3*-KO mice

After observing a significant reduction in levels of compulsive grooming behavior in *Sapap3*-KO mice following 7 days of fluoxetine administration, we assessed *in vivo* calcium activity from experimental day 7 and compared with calcium activity data from baseline day of the experiment to investigate potential neural correlates of effective SSRI treatment. Following the same process described in Sections 2.1.7.1 and 2.1.7.2, we aligned cells across days and compared the activity of each SPN at the onset of a grooming bout on experimental baseline day and experimental day 7. Only cells that were detected on both days of the experiment were included in subsequent analysis.

Figure 3.7A shows the distribution of groom onset-modulated SPNs in a single animal at baseline and on day 7. After matching cells, we separated out all units that were activated at baseline and assessed their subsequent activity on day 7 in each group. We found that there was a main effect of genotype on percentage of activated cells on day 7 relative to baseline day ($F(1,8) = 18.80$, $p = .0025$) and a main effect of FLX treatment ($F(1,8) = 7.8$, $p = .0235$). There was also an interaction between genotype and FLX treatment ($F(1,8) = 2.167$, $p = .1792$). Post hoc comparisons showed that 7 days of FLX treatment significantly reduced percentages of activated cells on day 7 relative to baseline day in KO mice (Figure 3.7B; $t(8) = 3.016$, $p = .0331$) but not WTs ($t(8) = .9339$, $p = .6127$).

When assessing the percentage of groom onset-inhibited cells in KOs and WTs at baseline and following 7 days of FLX treatment, there was no evidence for an effect of genotype or FLX treatment on the percentage of groom onset-inhibited cells ($F(1,8) = .3836$, $p = .5529$; $F(1,8) = .3008$, $p = .5936$). There was no interaction between genotype and FLX treatment on percentage of inhibited cells on day 7 relative to baseline day ($F(1,8) = .1763$, $p = .6856$).

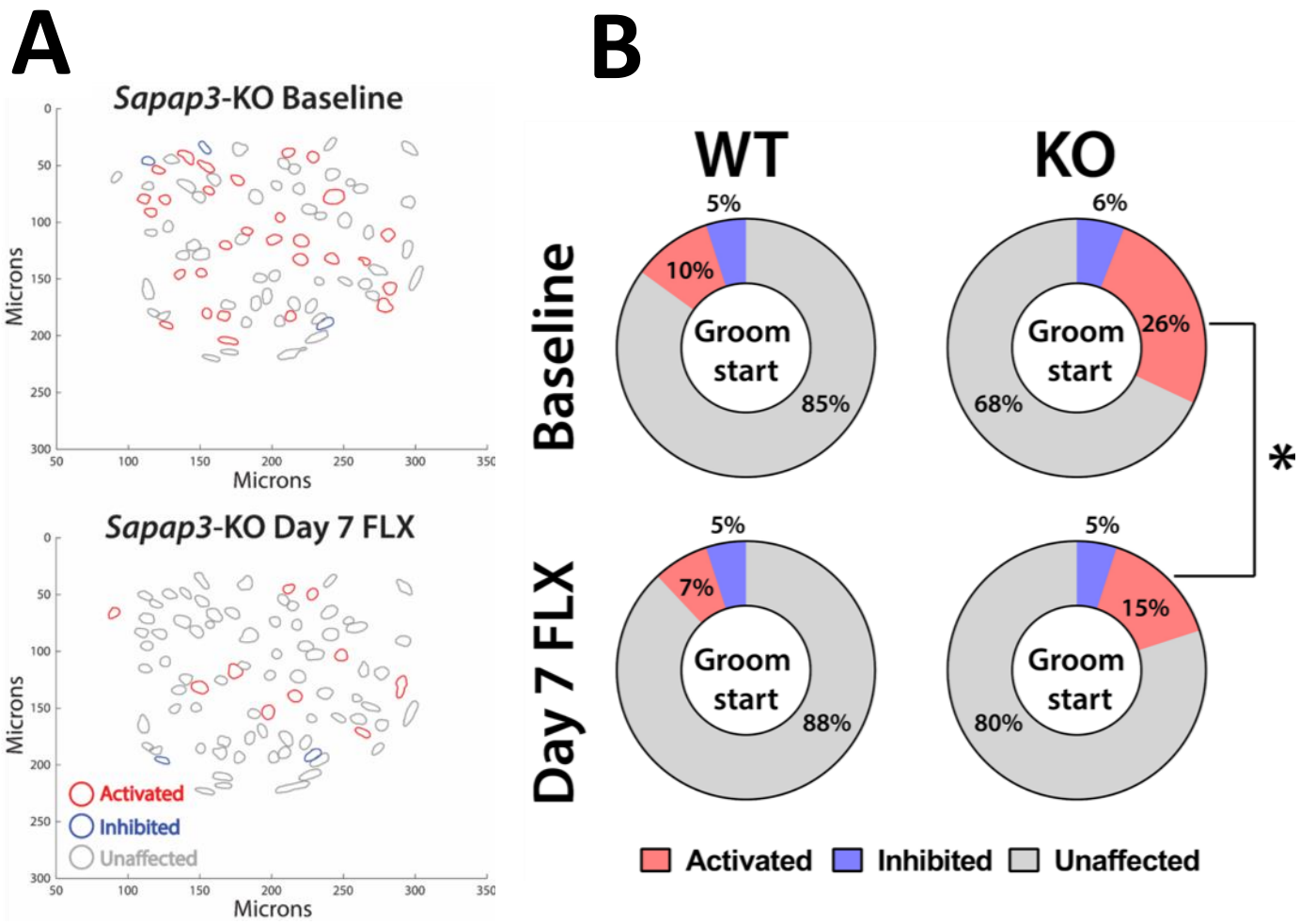

Figure 3.7 Percent of cells activated or inhibited by grooming at baseline and following 7 days flouxetine treatment.

(A) A representative sample of SPNs from the same KO mouse that were identified as activated by grooming onset on experimental baseline day. Of those found to be activated at baseline, some were found to be inhibited or unaffected by grooming onset after 7 days of fluoxetine treatment, while some cells maintained their categorization as grooming onset-activated SPNs. (B) At baseline, KO mice had a significantly higher percentage of groom onset-activated SPNs, relative to WT mice. Following 7 days of fluoxetine treatment, there was a significant reduction in the percentage of groom onset-activated SPNs in KO mice, while there was no significant change in the percentage of grooming-modulated SPNs observed in WT mice. 7 days of fluoxetine treatment did not significantly alter the percentage of groom onset-inhibited SPNs in either group (*$p < .05$).

3.2 Experiment 2 Results (D1-cre Cohort)

After observing overall hyperactivity within the striatum of *Sapap3*-KO mice relative to WT littermates at grooming onset, we were interested in investigating the activity of individual SPN subpopulations. In this experiment, we studied the grooming behavior of six D1-cre x *Sapap3*-KOs and eight D1-cre x *Sapap3*-WTs before and after 7 days of fluoxetine treatment. During each testing session, we also recorded calcium imaging data to investigate the grooming-associated activity of D1-SPNs in each group. We hypothesized that the striatal hyperactivity observed at grooming onset in *Sapap3*-KOs observed in Experiment 1 was driven by increased gain of D1-SPNs that would be evidenced by greater normalized fluorescence at grooming onset in D1-SPNs of D1-cre x *Sapap3*-KO mice relative to D1-cre x WT littermates.

3.2.1 D1-cre x *Sapap3*-KO mice groom more than D1-cre x *Sapap3*-WT mice

Previously it has been reported that *Sapap3*-KO mice spend significantly more time grooming than WT littermates (Welch et al. 2007). Here, we confirmed that crossing heterozygous *Sapap3* mutants (*Sapap3*$^{+/-}$) with D1-cre mice does not alter the grooming phenotype of *Sapap3*-KOs. Relative to D1-cre x WT littermates, D1-cre x *Sapap3*-KOs spent a significantly longer time engaged in grooming throughout a 40-minute testing session (Fig3.8A; $t(12) = 3.13$, $p = 0.0087$), and *Sapap3*-KOs performed more individual grooming bouts that WT counterparts (Fig. 3.8B; $t(12) = 2.991$, $p = 0.0113$).

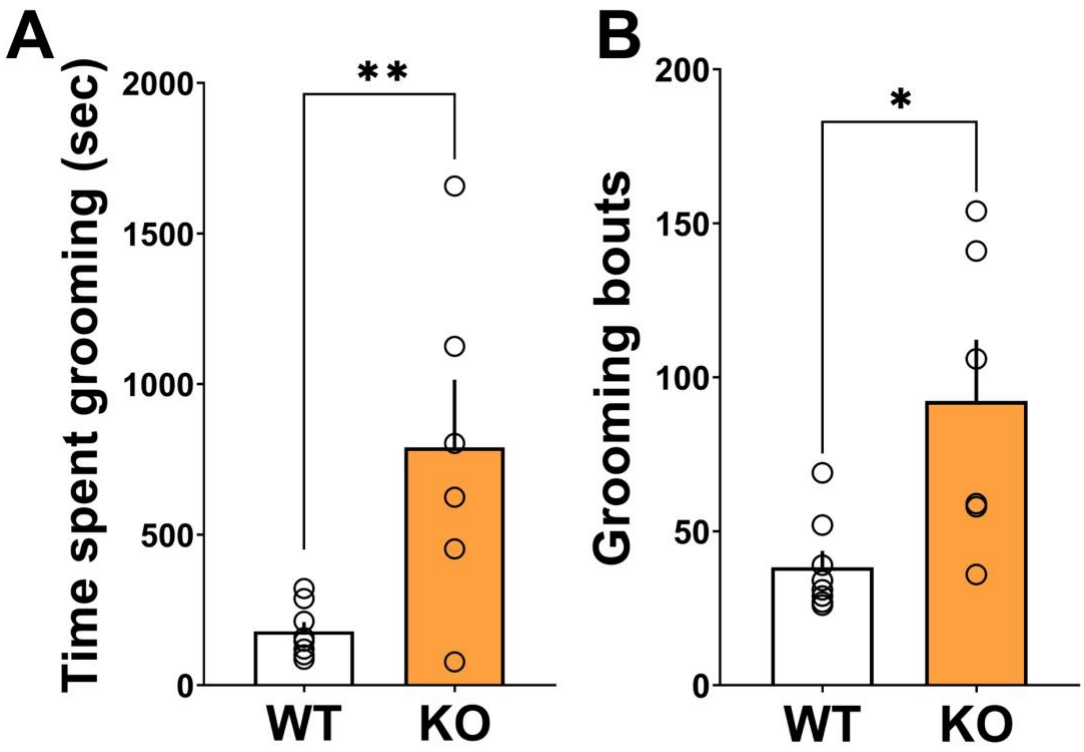

Figure 3.8 Total Grooming Time and Number of Grooming Bouts

(A) D1-cre x *Sapap3*-KO mice spent significantly more time grooming during 40-minute testing session relative to WT mice. (B) D1-cre *Sapap3*-KO mice initiated a significantly higher number of grooming bouts throughout the course of the session relative to WT mice. (**$p < .01$, *$p < .05$)

3.2.2 Altered amplitudes of grooming onset-modulated D1-SPNs in *Sapap3*-KOs relative to WT mice

As explained in Section 3.1.3, several underlying factors could contribute to genotype differences in grooming-associated calcium activity. One possibility is that *Sapap3*-KOs and WTs have equal numbers of grooming-modulated D1-SPNs, but the amplitudes of these cells differ across genotype. To investigate this possibility, we assessed the amplitude of activity-modulated D1-SPNs in each group. We categorized all D1-SPNs in each group as activated, inhibited, or unaffected by grooming-onset using the strategy described in Section 2.1.7.1. After separating out all activated units in *Sapap3*-KOs and WTs, we averaged across all activated units within each genotype. We also separated out all inhibited units in *Sapap3*-KOs and WTs and averaged across all inhibited units within each genotype.

When comparing the average amplitude of activated units across genotype, we found that the amplitude of normalized fluorescence of groom onset-activated D1-SPNs was significantly reduced in *Sapap3*-KO mice relative to WT counterparts at grooming onset and for several hundred milliseconds afterward. For groom onset-activated D1-SPNs, all significant time bins had t-values ≥ 4.2051 and p-values ≤ 0.000040519 (Fig. 3.9A; critical value after adjusting for multiple comparisons using Bonferroni, $p = 0.00005$). When comparing the average amplitude of inhibited units of D1-cre x *Sapap3*-KOs and D1-cre x WTs, we found that the amplitude of normalized fluorescence of groom onset-inhibited D1-SPNs was significantly increased in *Sapap3*-KOs relative to WT littermates, beginning roughly 1s after grooming onset. For grooming onset-inhibited D1-SPNs, all significant time bins had t-values ≥ 4.2134 and p-values ≤ 0.000046491 (Figure 3.9B; critical value after adjusting for multiple comparisons using Bonferroni, $p = 0.00005$).

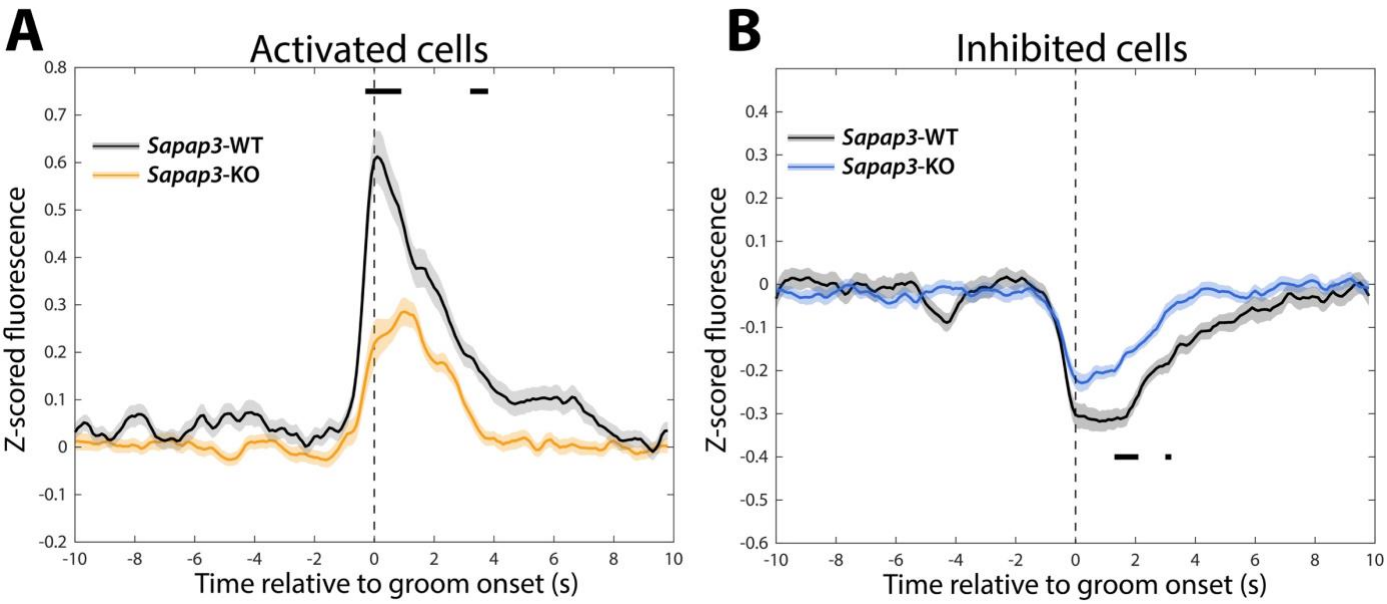

Figure 3.9 Amplitude of normalized fluoresence of grooming onset-activated D1-SPNs and grooming onset-inhibited D1-SPNs in *Sapap3*-KOs and WTs

This figure shows normalized calcium fluorescence of all D1-SPNs that are modulated by grooming-onset in D1-cre x *Sapap3*-KO and D1-cre x WT mice. (A) Z-scored fluorescence of groom onset-activated D1-SPNs of D1-cre x *Sapap3*-KO mice is significantly reduced relative to D1-cre x WT counterparts (bar indicates all $t \geq 4.2051$ and $p \leq 0.000040519$). (B) Z-scored fluorescence of groom onset-inhibited D1-SPNs of D1-cre x *Sapap3*-KO mice is significantly increased approximately 1s after grooming initiation, relative to D1-cre x WT littermates (bar indicates all $t \geq 4.2134$ and $p \leq 0.000046491$).

3.2.3 *Sapap3*-KO mice have more groom onset-inhibited D1-SPNs relative to WT littermates

In addition to differences in amplitude of grooming-modulated SPNs in *Sapap3*-KO mice, we hypothesized that there was a difference in the percent of grooming onset-activated and grooming onset-inhibited SPNs in *Sapap3*-KOs relative to WT littermates (similar to our findings in Experiment 1). Using the cell sorting methods described in Section 2.1.7.1, we assessed the activity-modulation of all SPNs in each group. We found that a significantly higher percent of total D1-SPNs were inhibited by grooming onset in *Sapap3*-KO mice relative to WT mice (Figure 3.10; $t(11) = 2.568$, $p = 0.0261$). There was no significant difference in the percentage of D1-SPNs activated by grooming onset across genotype (Figure 3.10; $t(11) = 0.0344$, $p = 0.9731$).

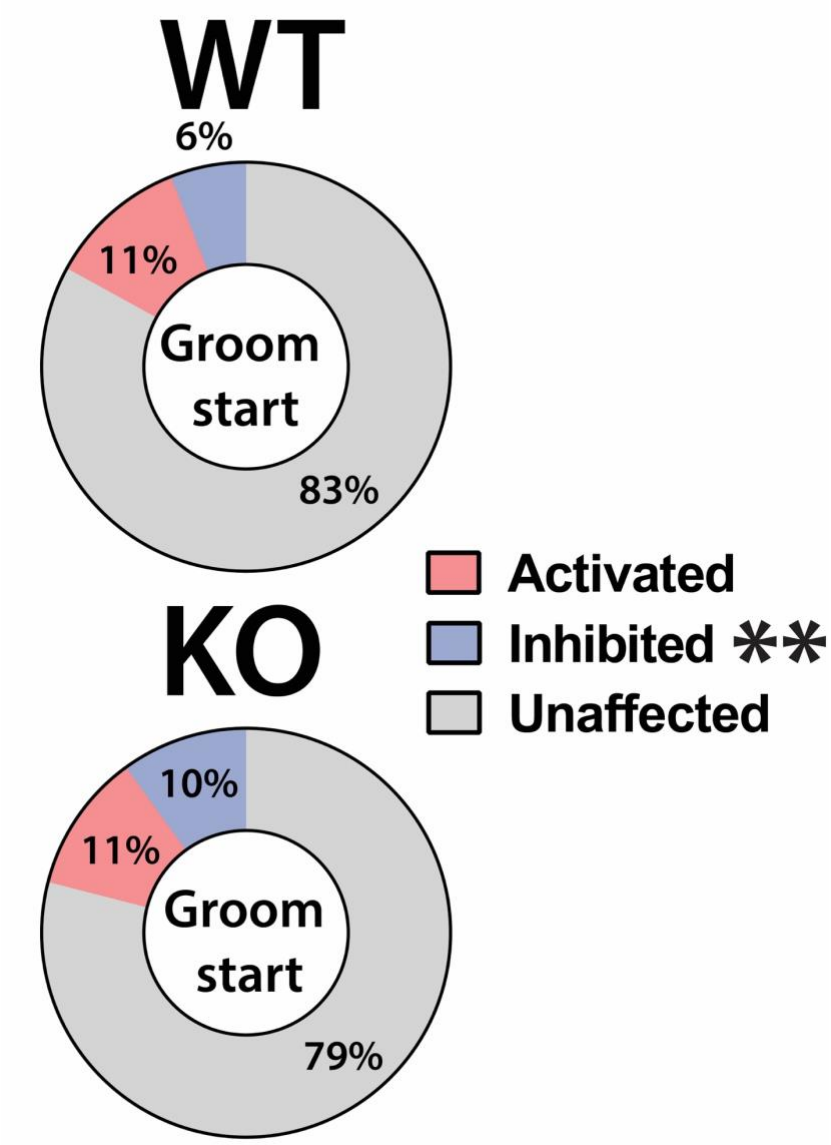

Figure 3.10 Grooming-Modulated D1-SPN Populations in *Sapap3*-KOs and WTs

A significantly higher percentage of groom onset-inhibited D1-SPNs were observed in *Sapap3*-KOs relative to WT mice. There was no significant difference in percentage of groom onset-activated D1-SPNs. (**$p < .001$)

3.2.4 Fluoxetine reduces compulsive grooming in D1-cre x *Sapap3*-KO mice

Following the baseline day of Experiment 2 in which behavior and *in vivo* calcium activity were recorded from D1-cre x *Sapap3*-KO and D1-cre x WT mice throughout a 40-minute testing session, all mice received 5mg/kg fluoxetine (FLX) in a .9% saline solution (10mL/kg) injected i.p. daily for 7 consecutive days. After completion of 7 days of fluoxetine treatment, grooming behavior and *in vivo* calcium activity were recorded throughout a second 40-minute testing session.

On day 7, we found that there was a main effect of genotype on time spent grooming ($F(1,11) = 6.988$, $p = 0.0228$) as well as a main effect of FLX treatment ($F(1,11) = 9.469$, $p = 0.0105$). Additionally, there was an interaction between genotype and FLX treatment ($F(1,11) = 5.940$, $p = 0.0330$). Post hoc comparisons showed that 7 days fluoxetine treatment significantly reduced time spent grooming in D1-cre x *Sapap3*-KO mice **(**Figure 3.11A; $t(11) = 3.757$, $p = 0.0063$) but not in D1-cre x WT mice (Figure 3.11A; $t(11) = 0.4710$, $p = 0.8753$). We also found a main effect of genotype on grooming bout number ($F(1,11) = 8.121$, $p = 0.0158$) as well as a main effect of FLX treatment ($F(1,11) = 5.467$, $p = 0.0393$) and an interaction between genotype and FLX treatment ($F(1,11) = 2.395$, $p = 0.1500$). Post hoc comparisons showed that 7 days of fluoxetine significantly reduced number of grooming bouts initiated by D1-cre x *Sapap3*-KO mice (Figure 3.11B; $t(11) = 2.648$, $p = 0.0448$) but not WT mice (Figure 3.11B; $t(11) = 0.5820$, $p = 0.8171$).

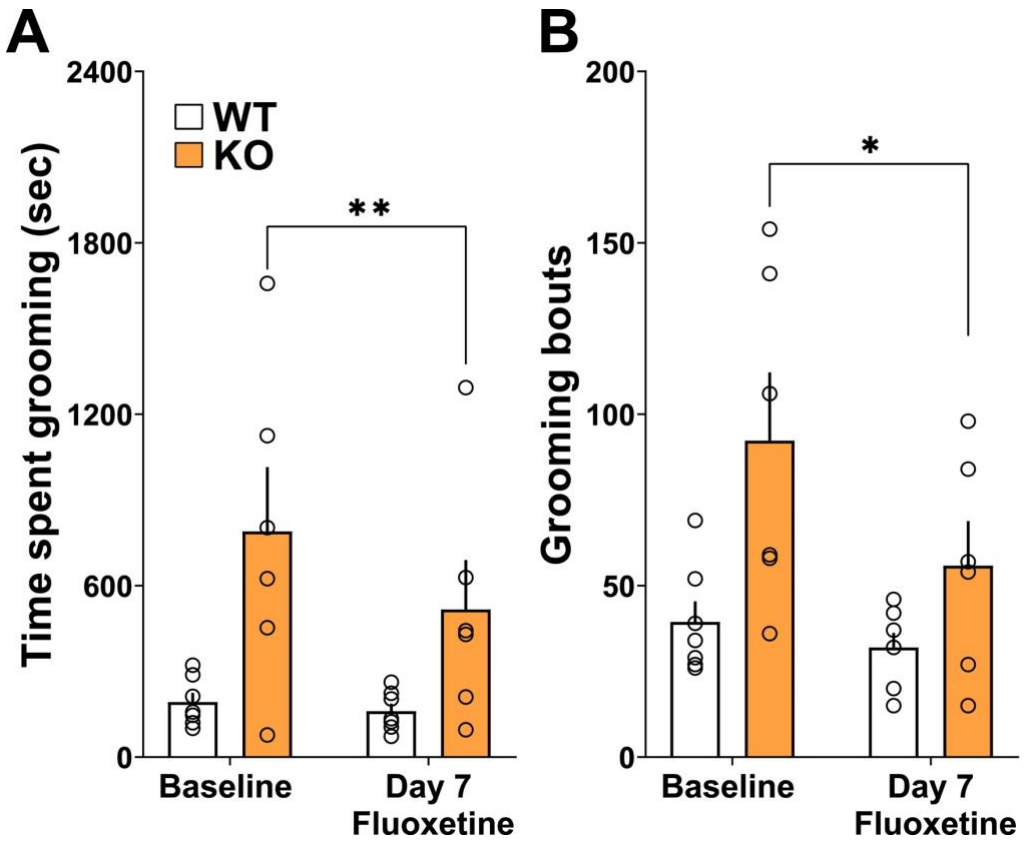

Figure 3.11 Grooming Time and Bout Number at Baseline and Following 7 Days Fluoxetine Treatment

(A) At baseline, D1-cre x *Sapap3*-KO mice spent a significantly longer time grooming in a 40-minute session relative to D1-cre x WT mice and initiated significantly more individual grooming bouts. Following 7 days of fluoxetine administration, grooming was significantly reduced in D1-cre x *Sapap3*-KO mice, but grooming levels of D1-cre x WT mice were unaffected. (B) At baseline, D1-cre x *Sapap3*-KO mice engaged in a significantly higher number of grooming bouts relative to D1-cre x WT littermates. After 7 days of fluoxetine administration, D1-cre x *Sapap3*-KO mice had a significant reduction in grooming bout number. These findings indicate that fluoxetine is capable of reducing compulsive grooming in D1-cre x *Sapap3*-KO mice and that drug administration does not affect activity of D1-cre x WT animals (**$p < .01$, *$p < .05$).

3.2.5 Minor increase in amplitude of groom onset-activated D1-SPNs of *Sapap3*-KOs following 7 days fluoxetine administration

After observing a significant reduction in levels of compulsive grooming behavior in *Sapap3*-KO mice following 7 days of fluoxetine administration, we assessed *in vivo* calcium activity from D1-SPNs on experimental day 7 to investigate potential neural correlates of effective SSRI treatment. Following the same procedure described in Section 2.1.7.1, we assessed the normalized fluorescence of all D1-SPNs in *Sapap3*-KOs and WTs at grooming onset. We compared the amplitude of normalized fluorescence of groom onset-activated and groom onset-inhibited D1-SPNs on before and after 7 days of fluoxetine administration. Note that on this day, in contrast to in Experiment 1, all grooming-modulated SPNs were considered, rather than only assessing changes in SPNs that were modulated by grooming onset on the baseline day.

We observed a significant increase in the amplitude of normalized fluorescence in groom onset-activated D1-SPNs in *Sapap3*-KOs (Fig. 3.12A; critical value after adjusting for multiple comparisons using Bonferroni, $p = 0.00005$), but no significant alterations in amplitude of grooming onset-activated D1-SPNs in WT animals. For grooming onset-activated D1-SPNs in *Sapap3*-KOs, all significant time bins had $t(151) \geq 4.1851$, $p \leq 0.0000482$. For grooming onset-activated D1-SPNs in WTs, amplitude difference closest to significant was $t(141) = 4.0643$, $p = 0.0000797$.

The normalized fluorescence of grooming onset-inhibited D1-SPNs was unaffected by SSRI administration in both groups. For groom onset-inhibited D1-SPNs in *Sapap3*-KO mice, the amplitude difference closest to significance was $t(122) = 3.467$, $p = 0.0007274$. For groom onset-inhibited SPNs in WT mice, the amplitude difference closest to significance was $t(95) = 3.260$, $p = 0.000965$.

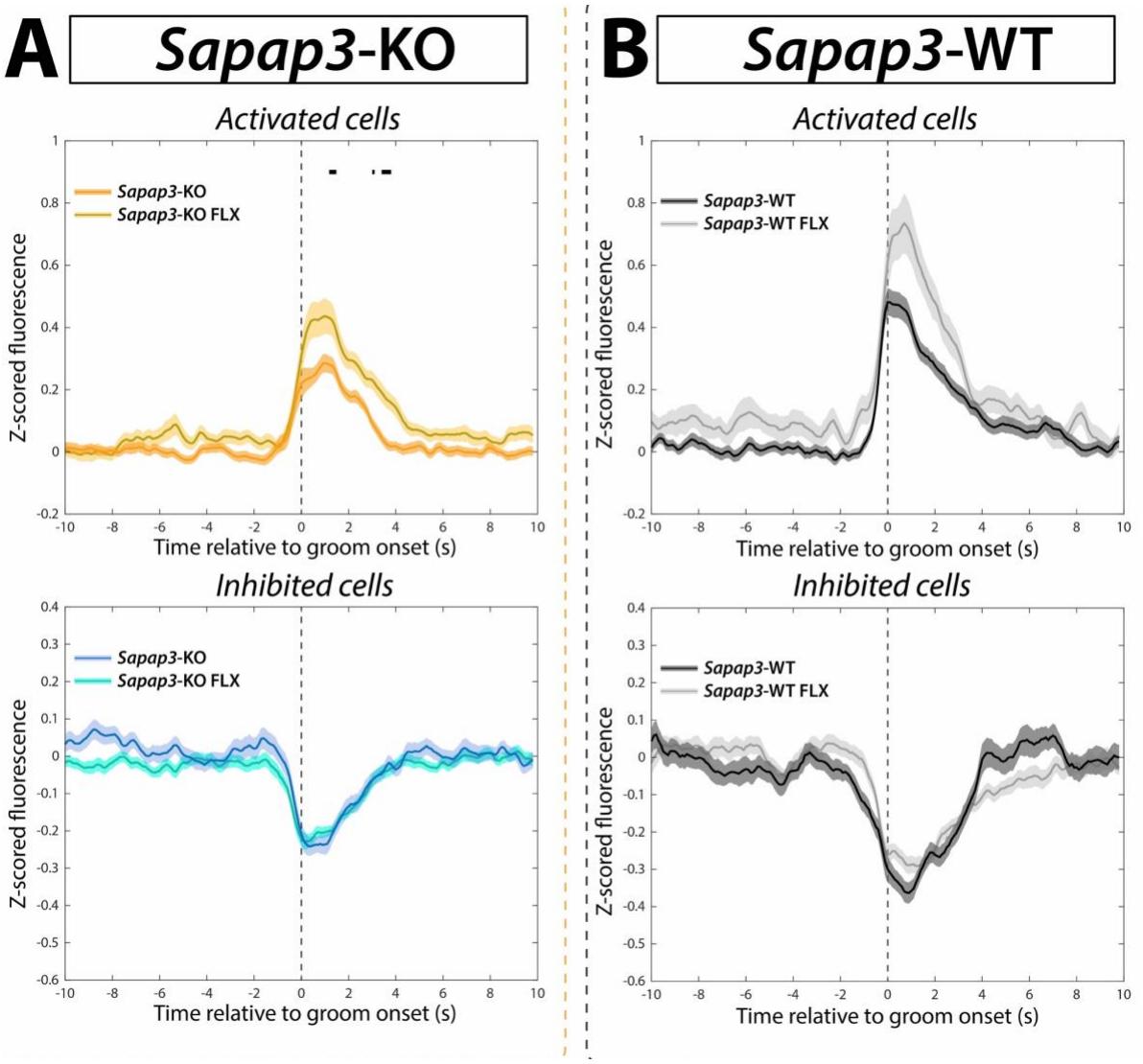

Figure 3.12 Amplitudes of Grooming-Modulated D1-SPNs Following 7 Days Fluoxetine Administration

This figure shows the normalized calcium fluorescence of all grooming-modulated D1-SPNs in *Sapap3*-KO and WT mice prior to and following 7 days fluoxetine administration. (A top) Following 7 days fluoxetine administration, there is a significant increase in amplitude of groom onset-activated D1-SPNs in *Sapap3*-KOs (bar indicates all $t(151) \geq 4.1851$, $p \leq 0.0000482$). (A bottom) Fluoxetine treatment did not affect normalized fluorescence of groom onset-inhibited D1-SPNs in *Sapap3*-KO mice (all $t(122) \leq 3.467$, $p \geq 0.0007274$). (B top) Fluoxetine treatment did not affect normalized fluorescence of groom onset-activated D1-SPNs in WT mice (all $t(141) \leq 4.0643$, $p \geq 0.0000797$). (B bottom) Fluoxetine treatment did not affect normalized fluorescence of groom onset-inhibited D1-SPNs in WT mice (all $t(95) \leq 3.260$, $p \geq 0.000965$).

3.2.6 Fluoxetine does not alter percentages of grooming-modulated D1-SPNs in *Sapap3*-KOs or WTs

In addition to comparing the amplitudes of grooming-modulated D1-SPNs following 7 days of fluoxetine administration, we investigated potential changes in the percentage of groom-onset activated and inhibited D1-SPNs across genotype after FLX treatment. As described in Section 2.1.7.1, we assessed the normalized fluorescence of all D1-SPNs at grooming onset on the experimental baseline day and experimental day 7.

When assessing the percentage of grooming onset-activated D1-SPNs following 7 days of fluoxetine treatment, there was no evidence for an effect of genotype or FLX treatment on the percentage of activated cells ($F(1,11) = 0.4483$, $p = 0.5170$; $F(1,11) = 1.381$, $p = 0.2648$). There was no interaction between genotype and FLX treatment on percentage of activated cells ($F(1,11) = 0.8773$, $p = 0.3691$).

When assessing percentages of grooming onset-inhibited D1-SPNs in *Sapap3*-KOs and WTs following 7 days fluoxetine treatment, we found that there was a main effect of genotype ($F(1,11) = 5.211$, $p = 0.0043$). There was no evidence for an effect of FLX treatment ($F(1,11) = 0.5344$, $p = 0.480$). There was no interaction between genotype and FLX treatment ($F(1,11) = 0.086$, $p = 0.7754$).

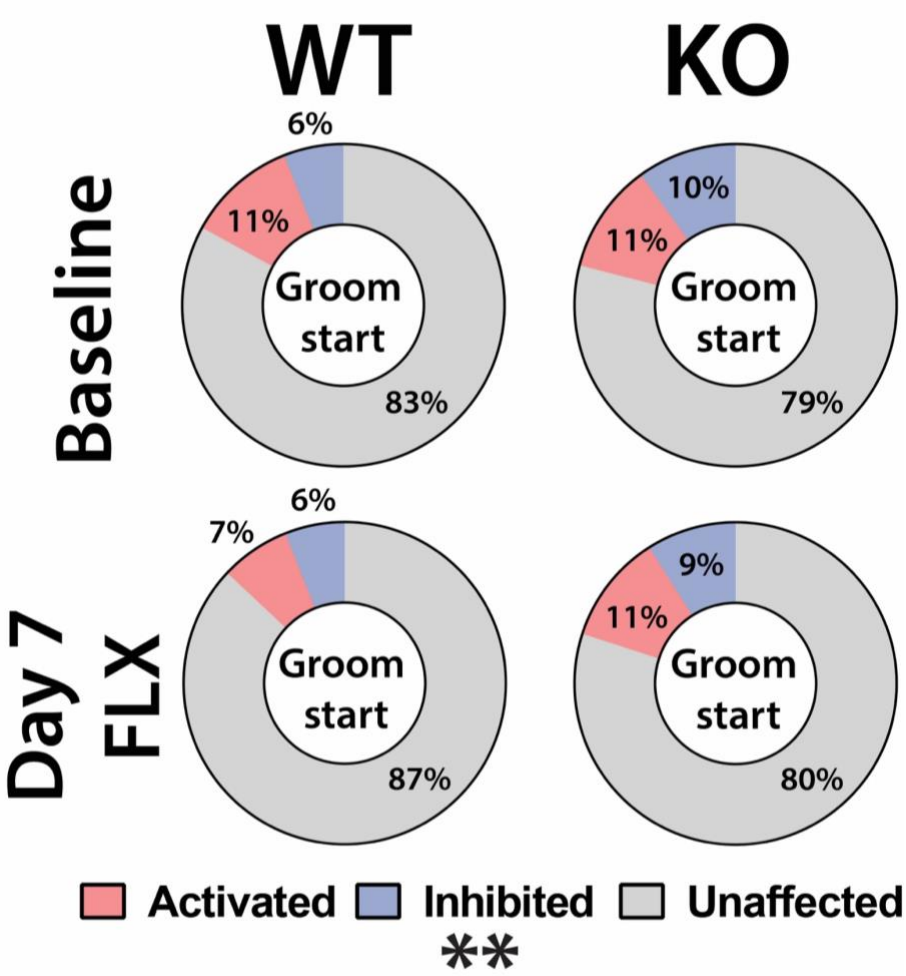

Figure 3.13 Percent of Grooming-Modulated D1-SPNs Following 7 Days Fluoxetine Treatment

At baseline and following 7 days fluoxetine treatment, *Sapap3*-KO mice had a significantly higher percent of groom-onset inhibited D1-SPNs relative to WT mice. There was no effect of genotype of FLX treatment on percent of groom-onset activated D1-SPNs (**$p < .001$).

4.0 DISCUSSION

In the present study, we sought to investigate the neural underpinnings of compulsive behaviors and to assess how successful SSRI treatment alters neural activity and behavior *in vivo*. We found that relative to WT counterparts, *Sapap3*-KO mice spent a significantly longer time grooming and engaged in a significantly higher number of grooming bouts in a 40-minute testing session. Following 7 days of fluoxetine treatment, grooming time and bout number were significantly reduced in *Sapap3*-KOs but unaffected in WTs. Using *in vivo* calcium imaging in this cohort, we observed a significant increase in normalized fluorescence in SPNs of *Sapap3*-KOs at grooming onset that was not observed in SPNs of WT mice. After categorizing all SPNs in each group as groom onset-activated, groom onset-inhibited, or groom onset-unaffected, we found that this effect was driven by recruitment of a greater number of groom onset-activated SPNs in *Sapap3*-KO mice compared to WT mice. Following 7 days of fluoxetine treatment, there was a significant reduction in the percent of groom onset-activated SPNs in *Sapap3*-KOs, while percentage of grooming-modulated SPNs was unchanged in WT mice.

After studying the combined activity of D1- and D2-SPNs *in vivo*, we specifically investigated the grooming-associated calcium activity of D1-SPNs using D1-cre x *Sapap3*-KO mice and D1-cre x WT mice. In this cohort, *Sapap3*-KO animals again spent a significantly longer time grooming and engaged in a significantly higher number of grooming bouts relative to WT mice, and this compulsive grooming behavior was significantly reduced in *Sapap3*-KO animals following 7 days of fluoxetine administration. Surprisingly, upon investigating *in vivo* activity of D1-SPNs at grooming onset, we observed a significant reduction in activity of D1-SPNs in *Sapap3*-KOs relative to WTs as measured by normalized calcium fluorescence. This striatal

hypoactivity could be explained by our observation of decreased amplitude of groom onset-activated D1-SPNs and an increase in the percent of groom onset-inhibited D1-SPNs. While compulsive grooming behavior was significantly reduced in *Sapap3*-KOs following 7 days of fluoxetine treatment, treatment had minor effects on D1-SPN activity. We observed a small, yet significant increase in normalized calcium fluorescence of groom onset-activated D1-SPNs in *Sapap3*-KOs, but no significant changes in the percent of grooming-modulated D1-SPNs in either group after fluoxetine administration.

4.1 Synthesizing Findings with Existing Literature

Our observations of baseline striatal hyperactivity at groom onset that was normalized following fluoxetine treatment in *Sapap3*-KO mice are consistent with previous reports that implicate the striatum in compulsive grooming in *Sapap3*-KOs. Specifically, it has been shown that *Sapap3*-KOs that received injection of a lentiviral vector that expressed GFP-SAPAP3 fusion protein in striatum on postnatal day 7 did not develop a compulsive grooming phenotype (Welch et al. 2007), suggesting that expression of SAPAP3 in striatum alone is sufficient to relieve the compulsive grooming that normally develops in *Sapap3*-KO mice.

In another study, synaptic transmission of SPNs was examined in *Sapap3*-KO mice through *ex vivo* electrophysiological recordings. AMPAR-mediated excitatory transmission in *Sapap3*-KOs was significantly reduced relative to WT littermates, but no differences in the presynaptic release probability of striatal SPNs were observed across genotype (Wan, Feng, and Calakos 2011). This lack of difference in presynaptic properties also points to striatal dysfunction in *Sapap3*-KOs, rather than upstream abnormalities.

As the striatum receives excitatory inputs from cortex and thalamus that differentially contribute to behavior (Wan et al. 2014; Pennartz et al. 2009), a follow-up study assessed AMPAR activity in corticostriatal and thalamostriatal synapses in *Sapap3*-KO mice to investigate if the striatal alterations observed in *Sapap3*-KOs is circuit-selective. Here, they found corticostriatal synaptic deficits but not thalamostriatal synaptic deficits in SPNs of *Sapap3*-KO mice and showed that SPNs have differential composition of SAPAP proteins at postsynaptic densities according to neural circuitry (corticostriatal vs thalamostriatal circuit) (Wan et al. 2014). These findings suggest that corticostriatal dysfunction driven by postsynaptic alterations underlies the compulsive grooming phenotype of *Sapap3*-KOs. Further support for this idea stems from recently published

work from our lab (Corbit et al. 2019), which demonstrates post-synaptic strengthening of inputs from M2 to central striatum in *Sapap3*-KOs using *ex vivo* electrophysiology. Additionally, *in vivo* electrophysiological recording showed a significant elevation in the baseline firing rates of striatal SPNs in *Sapap3*-KOs relative to WT littermates (Burguiere et al. 2013).

Building on this past work, we expanded upon the finding of baseline striatal hyperactivity in *Sapap3*-KOs to determine the temporal relationship between increased striatal activity and compulsive grooming behavior. Using *in vivo* calcium imaging, we demonstrated a significant increase in normalized fluorescence of the combined population of D1- and D2-SPNs in *Sapap3*-KO mice at grooming onset. Further, we demonstrated that this overall elevation in SPN activity was comprised of increased recruitment of SPNs activated at grooming onset in *Sapap3*-KO mice (as opposed to increased amplitude of groom onset-activated SPNs), a finding that was previously difficult to observe given the lower yield of cells captured using traditional electrophysiological recordings (e.g. 76-105 total units across all mice in central striatum (Burguiere et al. 2013), compared to over one hundred units per mouse on average in the present studies).

The literature predicts that an increase in overall striatal gain contributes to habit formation and expression (O'Hare et al. 2016; Cui et al. 2013), which has long been hypothesized to be involved in the pathophysiology of OCD (Graybiel and Rauch 2000). Specifically, it has been hypothesized that this increase in striatal gain hastens action onset at the cost of increasing outcome errors (Cui et al. 2013). Reinforcement of initially healthy habits under maladaptive conditions can lead to the development of compulsions, such as those performed by patients with OCD. Given the temporal link between habit expression and increased striatal gain in healthy conditions, it is possible that a further increase in striatal gain could drive the initiation of compulsive behaviors, consistent with the findings of the present study. However, it is important to note that most work

investigating the link between striatal gain and habit formation has focused on corticostriatal circuits that encompass the medial prefrontal cortex (mPFC) and medial striatum (Smith et al. 2012), which is located adjacent to the central striatum. It is currently unclear what, if any, role the central striatum plays in encoding habit formation, but we can speculate that increased central striatal gain in *Sapap3*-KOs may contribute to the formation of habitual (and ultimately compulsive) behaviors in a similar manner to what has been described in other sub regions of striatum, i.e. medial striatum and dorsolateral striatum.

An outstanding question leading from this work is: How is the striatal hyperactivity we observed at grooming onset, which is specifically characterized by an increase in the number of activated cells, generated at a circuit level? Spiny projection neurons comprise approximately 95% of striatal neurons, and the remaining 5% of striatal neurons are inhibitory interneurons (Blomeley and Bracci 2009). One subclass of striatal inhibitory interneurons is GABAergic parvalbumin-positive (PV+) fast-spiking interneurons (FSIs). While FSIs represent less than 1% of all striatal neurons, their influence on the activity of spiny projection neurons is outsized (Berke 2011). Relative to SPNs, FSIs receive convergent inputs from a wider range of cortical regions and are more responsive to these inputs. As their name suggests, fast-spiking interneurons respond to this cortical input with brief, high-frequency bursts of activity, synapsing onto the soma or proximal dendrites of neighboring SPNs (Berke 2011). This stochastic GABAergic input onto many surrounding SPNs creates widespread feedforward inhibition of striatal activity. Because of the basal ganglia's critical role in action selection, this feedforward inhibition may enable selection of favorable actions while suppressing incompatible alternative actions (Owen, Berke, and Kreitzer 2018).

Evidence from the literature also supports the converse idea- i.e., weakening this feedforward inhibition onto SPNs could result in aberrant striatal activity and an inability to efficiently select an adaptive action. First, losing FSIs (and their associated inhibition of SPNs) has been associated with disorganized behavioral output. Specifically, several post-mortem studies have reported that, relative to healthy comparison subjects, there is a significant reduction (50-60%) in the number of PV+ interneurons in the striatum of patients with severe Tourette syndrome (TS) – a neuropsychiatric illness associated with motor and vocal tics that has a high incidence of comorbidity with OCD (Kataoka et al. 2010; Kalanithi et al. 2005). Preclinical studies have also suggested a role for FSIs in repetitive behaviors. In an attempt to recapitulate the anatomical changes observed in post-mortem tissue from TS patients, (Xu, Li, and Pittenger 2016) performed targeted ablation of striatal FSIs in mice. To remain as consistent with post-mortem literature as possible, they ablated roughly 50% of FSIs in dorsal striatum. They found a significant increase in performance of stress-induced grooming behavior in PV-ablated mice relative to control animals, indicating that reducing FSI activity is sufficient to increase repetitive grooming in mice (Xu, Li, and Pittenger 2016). Another study found that selective inhibition of striatal FSIs via local infusion of a GABA antagonist led to dyskinetic behavior in mice (Gittis et al. 2011). Interestingly, this selective FSI inhibition resulted in increases and decreases in striatal SPN firing rates, supporting the notion that striatal FSIs are responsible for coordinating the activation of striatal SPNs for adaptive action selection, rather than strictly inhibiting neighboring SPNs (Gittis et al. 2011). Similarly, a recent study showed that both optogenetic suppression and over-activation of striatal FSIs disrupted performance of reward anticipatory behavior (licking), indicating that under physiological conditions, FSIs modulate SPN activity to enhance behavioral performance (Lee et al. 2017).

In 2013, (Burguiere et al. 2013) observed a significant reduction in the number of striatal FSIs in *Sapap3*-KO mice relative to WT littermates and utilized optogenetics to examine if this loss of striatal feedforward inhibition played a causal role in the production of a compulsive grooming phenotype in *Sapap3*-KO mice (but see (Corbit et al. 2019) where no differences in PV+ cell numbers are observed between *Sapap3*-KOs and WTs). To do so, they optogenetically stimulated axon terminals from the lateral OFC (lOFC) in centromedial striatum and recorded from FSI-SPN pairs. Stimulation of ChR2-containing lOFC axon terminals resulted in a significant increase in activation of FSIs and subsequent increased inhibition of SPNs (Burguiere et al. 2013). Critically, they showed that lOFC axon terminal stimulation could rescue the compulsive grooming phenotype of *Sapap3*-KO mice. Compared to control *Sapap3*-KO animals injected with YFP, ChR2 stimulation of lOFC terminals in *Sapap3*-KO mice led to a significant reduction in grooming during laser on periods relative to laser off periods (Burguiere et al. 2013). Based on these findings, one possible explanation for the striatal hyperactivity we observed in *Sapap3*-KOs at grooming onset is a decrease in feedforward inhibition from neighboring FSIs.

Consistent with this prediction, unpublished work from the Ahmari lab indicates that in lOFC there is a significant reduction in normalized calcium fluorescence at grooming onset in *Sapap3*-KO mice relative to WT littermates. Specifically, this broad reduction in lOFC activity appears to be driven by an increase in the percentage of grooming onset-inhibited cells in *Sapap3*-KO animals. To complement these findings, a recent study from our lab showed that *ex vivo* optogenetic activation of lOFC terminals in WT mice resulted in preferential activation of striatal FSIs over SPNs (Corbit et al. 2019). With these data in mind, it is reasonable to speculate that striatal hyperactivity in *Sapap3*-KO mice at grooming onset is evoked by decreased lOFC activation of striatal FSIs, resulting in disinhibition of striatal spiny projection neurons.

4.1.1 Fluoxetine affects striatal activity *in vivo*

In addition to observing striatal hyperactivity *in vivo* in *Sapap3*-KO mice, we found that 7 days of fluoxetine treatment normalized striatal activity in *Sapap3*-KOs on the same timescale as behavioral normalization. It is currently unclear how fluoxetine affects corticostriatal circuitry *in vivo*. However, our findings are consistent with previous reports indicating that serotonin directly influences neuronal excitability. In one study, bath application of serotonin to rat brain slices strongly increased the excitability of striatal FSIs relative to control conditions (Blomeley and Bracci 2009). This effect was mediated by serotonin acting on the 5-HT_{2C} receptor that is highly expressed on FSIs. In a separate study, the effect of fluoxetine on FSI excitability was assessed directly. Firing rates of PFC FSIs and pyramidal neurons were recorded prior to and following bath application of fluoxetine to slices of rat cortex. Fluoxetine significantly increased single-cell firing rates of PFC FSIs in a dose-dependent manner but did not impact pyramidal cell firing rates (Zhong and Yan 2011). Furthermore, unpublished data from the Ahmari lab shows that single-cell firing rates of striatal FSIs are significantly increased following bath application of fluoxetine (Corbit, Gittis, & Ahmari, unpublished observations).

Considering this evidence, one rational explanation of the current findings is that fluoxetine decreases striatal activity at grooming onset by increasing the excitability of striatal FSIs. FSIs are then able to re-exert their modulatory influence on neighboring SPNs, restoring normal patterns of striatal activity. While further studies must be conducted to uncover the precise pharmacological mechanisms of SSRIs such as fluoxetine, the results of the present study provide support for the hypothesis that SSRIs effectively reduce maladaptive, aberrant behaviors by reestablishing the feedforward inhibition of FSIs onto SPNs in the striatum.

4.1.2 D1- and D2-SPN contributions to compulsive behaviors

Through the "direct pathway" of basal ganglia circuitry, D1-SPNs disinhibit the thalamus, enabling thalamus to send excitatory projections to cortex to direct the execution of movements, As *Sapap3*-KO mice groom excessively, we hypothesized that the overall striatal hyperactivity observed in Experiment 1 was driven by increased D1-SPN activity at grooming onset in *Sapap3*-KOs. Specifically, it is well-established that activating D1-SPNs with the dopamine 1 receptor agonist SKF induces excessive grooming in rodents in a dose-dependent manner (Stoessl 1994; Page SJ 1997; Deveney AM 1995). Furthermore, we speculated that the overall hyperactivity observed in *Sapap3*-KO mice may be driven by reduced input from striatal FSIs. A recent study conducted *ex vivo* electrophysiological recordings in striatal FSIs that synapsed onto D1- and D2-SPNs. They found that a significantly higher percent of FSI→D1-SPN pairs were functionally connected compared to FSI→D2-SPN pairs (Gittis et al. 2010). This apparent bias of FSI feedforward inhibition onto D1-SPNs also led us to hypothesize that D1-SPNs are responsible for the overall striatal hyperactivity observed in *Sapap3*-KO mice. Additionally, results of *in vivo* electrophysiological recordings in striatum of *Sapap3*-KO and WT mice show a shift in striatal output favoring the direct (D1) pathway in *Sapap3*-KO mice relative to WTs, providing further evidence that increased D1-SPN drive underlies the compulsive grooming behavior observed in *Sapap3*-KO mice (O'Hare et al. 2016). Finally, there have been several *ex vivo* electrophysiology studies from animal models supporting the idea that excessive activity in D1-SPNs is related to the development of abnormal repetitive behaviors. However, the results of Experiment 2 were not consistent with this hypothesis, because we observed a significant reduction in activity of D1-SPNs of *Sapap3*-KOs relative to WTs that was driven by an increased percentage of groom onset-inhibited D1-SPNs.

Given the findings of Experiments 1 and 2 presented in this thesis, it is likely that D2-SPN hyperactivity is responsible for the overall grooming-associated striatal hyperactivity observed in *Sapap3*-KO mice. While this may initially seem counterintuitive, several studies indicate that D2-SPN activity may be more relevant to the generation of compulsive behaviors than previously assumed**.** A recent study conducted by (Rothwell et al. 2015) investigated the role of direct and indirect corticostriatal pathways in behavioral performance on a serial order task. Optogenetic stimulation of D2-SPNs in DLS led to a decrease in the percentage of correct serial order trials, and optogenetic inhibition of D2-SPNs resulted in significant improvements in accurate completion of the task (Rothwell et al. 2015). Critically, D2-SPN stimulation did not alter the latency of responding, which contradicts the classical model that asserts that D2-SPN activation results in inhibition of movements, and specific studies that show optogenetic stimulation of D2-SPNs impedes movement (Kravitz et al. 2010). As *Sapap3*-KO mice display abnormally high levels of grooming behavior, it is possible that concomitant D2-SPN hyperactivity is responsible for this phenomenon.

Additional support for D2-SPN involvement in compulsive behaviors comes from clinical studies. Compared to healthy comparison subjects, OCD patients have decreased D2 receptor availability in striatum prior to receiving pharmacological treatment (Moresco et al. 2007). Decreased receptor availability likely results from increased activation of D2-SPNs and compensatory endocytosis of receptors. Following twelve weeks of treatment with the SSRI fluovamine, all but one OCD patient (from a group of 9 individuals) showed significant improvement in symptoms. Critically, PET scans showed that treatment responsive individuals had a significant increase in the D2 receptor availability in the striatum (Moresco et al. 2007). These findings provide further evidence that D2-SPN hyperactivity may be implicated in the

compulsive symptoms associated with OCD and lead us to hypothesize that striatal hyperactivity observed in *Sapap3*-KO mice during compulsive grooming is primarily driven by excessive D2-SPN activity.

4.2 Methodological Limitations

While the findings presented in this thesis provide novel insight into the neural correlates of compulsive behaviors, further investigation must be performed to more completely resolve the circuit-level mechanisms underlying compulsive grooming in our animal model. In particular, it is difficult to make strong claims regarding the cell-type specificity of grooming-associated striatal hyperactivity that we observed in *Sapap3*-KO mice without assessing the activity of D2-SPNs *in vivo*. Because generating double-transgenic mouse lines is a time-intensive process, we have made several attempts to investigate the *in vivo* calcium activity of D2-SPNs while breeding up a colony of A2A-cre x *Sapap3*-KO and A2A-cre *Sapap3*-WT mice.

First, we attempted to utilize a D2-specific promoter GCaMP6m virus (AAV8-D2R-GCaMP6m) to specifically label D2-SPNs in *Sapap3*-KOs. This virus was developed by the Deisseroth Lab in 2016 by cloning the D2-specific promoter fragment from rat genome, found immediately upstream of the D2 receptor gene (Zalocusky 2016). Because there has been no published use of this virus in mice, we first wanted to confirm D2-specific viral expression. To do so, we injected 800nl of this D2-GCaMP6m into central striatum of D1-tdTomato mice that express red fluorescent protein (RFP) in all D1 receptor-expressing SPNs. If this virus was truly D2-specific, we hypothesized that we would not observe colocalization of RFP and GFP in striatum of D1-tdTomato mice that received viral injection. We followed the same surgical procedures for surgery 1 described in Section 2.1.2, and waited four weeks to allow sufficient viral transfection. At this point, mice were sacrificed, and tissue was perfused for further analysis. I carefully examined 35µm slices that had been enhanced for GFP using immunohistochemistry under a confocal microscope. As hypothesized, we did not observe colocalization of RFP and GFP, suggesting that this virus is indeed specific for D2-SPNs.

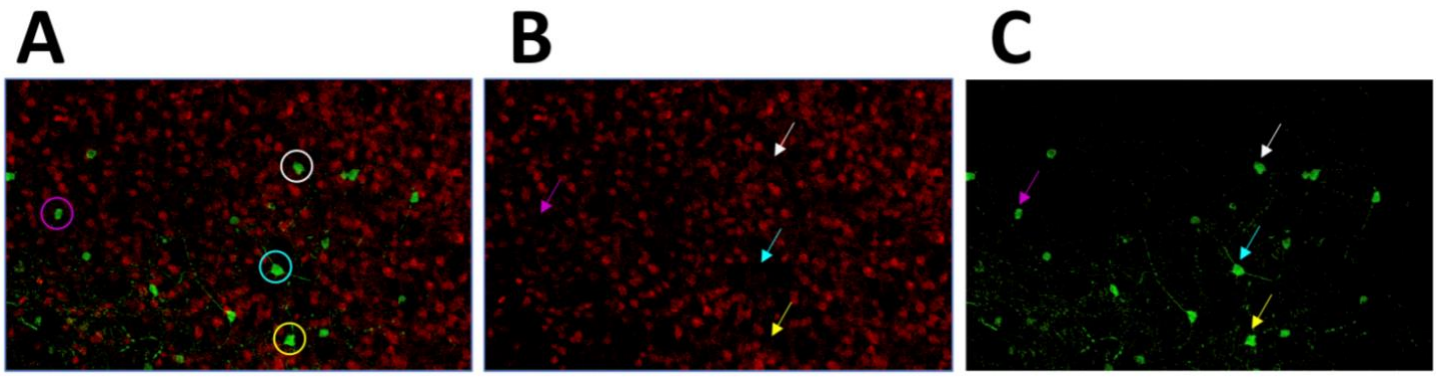

Figure 4.1 Representative Confocal Image of Striatum of D1-tdTomato Mouse with D2-SP-GCaMP Injection

(A) Merged image of RFP channel (showing all D1-SPNs) and GFP channel (showing SPNs infected with D2-SP-GCaMP virus). (B) RFP channel, showing all D1-SPNs. (C). GFP channel, showing all SPNs infected with D2-SP-GCaMP virus. We observed negligible RFP and GFP colocalization, indicating that the D2-SP-GCaMP virus is specific for D2-SPNs in mice.

While it was reassuring to observe viral specificity, we found that the efficacy of this virus for *in vivo* calcium imaging in mice was limited. Upon attaching the miniature microscope to surgerized animals to visualize *in vivo* calcium fluorescence from D2-SPNs, we unfortunately observed dim fluorescence that limited our ability to localize many individual SPNs. Over the course of several additional weeks we reassessed calcium fluorescence in these animals to ensure that our initial observations were not simply the result of insufficient viral transfection, but the calcium signal did not improve. Given these findings, this approach could not be used to achieve our experimental goal of assessing activity-related calcium activity of D2-SPNs *in vivo*.

After failing to observe sufficient *in vivo* calcium fluorescence from D2-SPNs with the D2-specific promoter GCaMP6m virus, we pursued an alternative strategy. As described in Section 1.1.3.1, the output structures of D1- and D2-SPNs diverge, forming the canonically-described

direct and indirect pathways of the basal ganglia. D1-SPNs specifically project to the internal segment of globus pallidus (GPi) and substantia nigra pars reticulata (SNr), while D2-SPNs project to the external segment of globus pallidus (GPe). Therefore, D2-SPNs could be specifically infected by injecting a retrograde GCaMP7 virus into the GPe. To assess the efficacy of this approach, I injected a retrograde GCaMP7 virus (retro-AAV-hSyn-GCaMP7, 1.85e13, addgene 104488) into the GPE of WT mice and waited a minimum of 5 weeks for the virus to be transported to D2-SPN cell bodies in the striatum. After 5 weeks, animals were sacrificed, and tissue was perfused. Brains were sliced at -20ºC into 35µm slices using a Leica CM3050 cryostat. Slices were mounted onto slides, cover-slipped with Fluoroshield™ DAPI mounting medium and visualized using a scanning microscope at 10x magnification. Surprisingly, in spite of consistent viral targeting of GPe, we did not see any GFP expression in striatum. We have therefore not been able to successfully visualize *in vivo* calcium activity of D2-SPNs with this experimental strategy. We look forward to complementing the investigation of D1-SPN activity presented in this thesis with an *in vivo* calcium imaging study in A2A-cre x *Sapap3*-KO and A2A-cre x *Sapap3*-WT mice in the coming months (to be discussed further in Section 4.3).

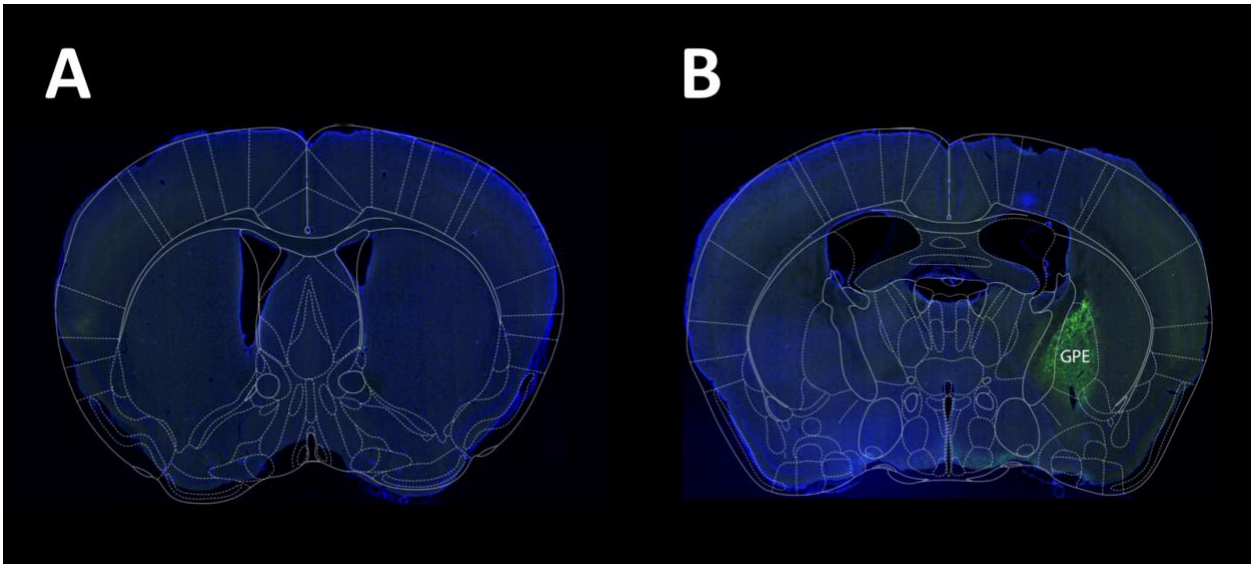

Figure 4.2 Representative Image of Striatum and GPe after Injection of Retro-GCaMP7

(A) Scanning microscope image at 10x magnification of striatum 5 weeks after retro-GCaMP7 injection into GPe. (B) Scanning microscope image at 10x magnification of GPe 5 weeks after retro-GCaMP7 injection into GPe. In spite of consistent viral targeting of GPe, we did not observe viral expression in striatum, a target input structure of GPe.

In the present study, we were limited in the number of groups we could include in each experiment. In particular, these experiments would have benefitted from having one additional group of each genotype that received vehicle injections of .9% saline instead of fluoxetine injections. It is possible that animals groomed less following 7 days of fluoxetine administration simply because they became more comfortable with experimenters after being scruffed and handled for 7 consecutive days. Comparing the behavior of *Sapap3*-KO + fluoxetine and *Sapap3*-KO + vehicle on day 7 would allow us to assess this possibility and could be insightful in guiding accurate interpretation of our data.

While we did not have vehicle groups, we recorded behavioral activity and *in vivo* calcium activity two weeks after the completion of fluoxetine treatment. Previous studies report comparable levels of grooming in *Sapap3*-KOs after two weeks of fluoxetine washout with

Sapap3-KOs that received vehicle treatment in place of fluoxetine (Ahmari et al. 2013). These data indicate that assessing behavioral and neural activity after a two-week washout period is a useful measure to consider in the absence of additional vehicle groups. However, even after analyzing the results of a two-week washout test, we cannot be certain that the effects we observe are necessarily caused by fluoxetine treatment rather than additional factors such as greater habituation to experimenters and behavioral conditions. Until our studies can be replicated with additional vehicle groups, we must consider the additional variables that could have contributed to the present findings.

4.3 Future Directions

The current work suggests several directions of future research. First and foremost, it is important to investigate the grooming-associated activity of D2-SPNs in *Sapap3*-KO and WT mice to complement the studies of D1-SPNs described in this thesis. We are currently breeding A2A-cre x *Sapap3*-KO and A2A-cre x *Sapap3*-WT mice, and we intend to perform surgeries on the first cohort in the coming months in order to directly assess the activity of D2-SPNs *in vivo.*

After completing thorough investigation of SPN activity in *Sapap3*-KO and WT mice, the next logical step is to examine the grooming-associated activity of striatal FSIs in *Sapap3*-KOs and WTs using *in vivo* calcium imaging. This will be achieved by injecting a Cre-dependent GCaMP6m virus (AAV-Syn-Flex-GCaMP6m-WPRE-SV40, 2.7e13) into striatum of PV-cre x *Sapap3*-KO and PV-cre x *Sapap3*-WT mice so that GCaMP will only be expressed in PV-positive cells. The surgical procedures will be similar to those described in this thesis with some minor modifications to account for the small population size of striatal FSIs (less than 1% of all striatal neurons). Specifically, we will implant a 1mm GRIN lens to maximize the number of FSIs we can image. Based on the findings presented in this thesis and our lab's work investigating *in vivo* calcium activity in lOFC of *Sapap3*-KO and WT mice, I hypothesize that normalized calcium fluorescence in FSIs at grooming onset will be reduced in *Sapap3*-KO mice relative to WT counterparts and that 7 days of fluoxetine administration will significantly increase calcium activity of *Sapap3*-KO FSIs at grooming onset. While it will be technically challenging to image from striatal FSIs *in vivo,* investigating grooming-associated FSI activity in *Sapap3*-KOs and WTs will provide informative confirmation or refutation of our working hypothesis that the striatal hyperactivity observed in *Sapap3*-KO mice is driven by a reduction of FSI feedforward inhibition

onto SPNs. In either case, these findings will bolster our understanding of how aberrant CTSC activity contributes to behavioral compulsivity.

In recent months, our lab has investigated the causal relationship between striatal hyperactivity and compulsive grooming using optogenetic stimulation of central striatal cell bodies. In this study, we utilized only WT mice. Animals were assigned to either an experimental or control group, receiving an injection of channelrhodopsin (ChR-2) or YFP in striatum. By intermittently stimulating CS cell bodies with blue light pulses, we see a significantly higher probability of grooming during light-on trials in ChR-2 mice compared to YFP mice. These data indicate that we can recapitulate grooming behavior by directly increasing striatal activity. I am interested in building upon these findings by performing a complementary experiment in *Sapap3*-KO mice using an inhibitory opsin, halorhodopsin, in place of channelrhodopsin. In this experiment, animals will either receive an injection of halorhodopsin or YFP into striatum. Given my findings thus far, I hypothesize that intermittently inhibiting central striatal cell bodies will significantly reduce probability of grooming during light-on trials in *Sapap3*-KO mice. Further optogenetic manipulation of this circuitry in *Sapap3*-KO and WT mice will allow us to make stronger claims about the causal relationship between circuit-level abnormalities in striatum and compulsive behavior that can only be inferred from *in vivo* calcium imaging studies.

Ultimately, I hope to attain comprehensive answers to the scientific questions posed in the Ahmari lab by combining *in vivo* calcium imaging and optogenetics. In (Burguiere et al. 2013), stimulation of lOFC axon terminals in striatum of *Sapap3*-KO animals significantly reduced probability of grooming during light-on trials. The authors hypothesized that this effect was caused by increased lOFC excitation of striatal FSIs and subsequent inhibition of striatal SPNs. However, this was not observed directly. Using new Inscopix nVoke technology that enables simultaneous

optogenetic manipulation and *in vivo* calcium imaging, the mechanism underlying this effect can be investigated in a more definitive manner. By injecting a red-shifted opsin such as Chrimson (Klapoetke et al. 2014) in lOFC and a Cre-dependent GCaMP6m virus (AAV9-Syn-Flex-GCaMP6m-WPRE-SV40, 2.7e13) in striatum of PV-cre x *Sapap3*-KO, I will directly observe the effect of lOFC axon terminal stimulation on FSI activity. Based on the findings of (Burguiere et al. 2013) and the supportive data that I have generated in this thesis, I hypothesize that lOFC terminal stimulation will decrease the probability of grooming during light-on trials in PV-cre x *Sapap3*-KO mice. Additionally, I hypothesize that lOFC stimulation will result in increased calcium fluorescence from striatal FSIs. A similar approach could be utilized in D1-cre x *Sapap3*-KO mice and A2A-cre x *Sapap3*-KO mice to investigate the effect of lOFC stimulation on D1- and D2-SPN activity. These experiments will provide deeper insight into the findings presented in the current study and guide the direction of further research.

4.4 Impact of Current Work

Despite the severity and high prevalence of obsessive compulsive disorder (OCD), there is limited understanding of the precise mechanisms underlying this disease. Coupled with this, current treatment methods for OCD have limited efficacy with only 25% of patients achieving full remission with the first line pharmacologic treatment (Goddard et al. 2008). Neuroimaging studies have consistently reported structural and functional abnormalities in CSTC circuits in OCD (Piras et al. 2015; Pujol et al. 2004; Rotge et al. 2009; Rauch 1994; Saxena 1999), but it is difficult to investigate neural circuit mechanisms in human subjects. Instead, we turn to translational animal models. *Sapap3*-KO mice provide a particularly useful model for investigating the circuit-level abnormalities that may underlie OCD symptoms. These mice display a compulsive grooming phenotype and abnormalities in corticostriatal neurotransmission. In addition, the compulsive grooming phenotype of *Sapap3*-KOs responds to fluoxetine treatment, making them a useful model for investigating how effective SSRI treatment influences neural activity in CSTC circuits. OCD is a heterogeneous disorder that undoubtedly cannot be simplified to altered expression of a single gene. With this in mind, it is interesting to note that in the first post-mortem study of differential gene expression in OFC and striatum of OCD subjects and matched comparison subjects, expression of the *DLGAP3* gene (synonymous with *Sapap3* in mouse genome) was significantly decreased both OFC and striatal regions in OCD subjects relative to matched comparison subjects (Piantadosi, et al. 2019, accepted, Molecular Psychiatry). This finding provides further support for the use of *Sapap3*-KO mice to probe the neural circuitry that has been implicated in OCD.

In this thesis, I reported that striatal hyperactivity observed in *Sapap3*-KO mice was driven by increased recruitment of spiny projection neurons at the onset of grooming. After 7 days of

fluoxetine treatment, the compulsive grooming phenotype of *Sapap3*-KO mice was significantly reduced, and there was a significant decrease in the percent of grooming onset-activated SPNs. These findings could potentially indicate that the broad striatal hyperactivity measured via PET and fMRI in OCD patients is the result of more individual cells being active, rather than a stronger upstream drive onto striatal neurons**.**

In addition to reducing the compulsive grooming behavior of *Sapap3*-KO mice with fluoxetine treatment, our lab has shown that 5 days of treatment with a 5-HT_{2C}-specific receptor agonist also significantly reduces grooming in *Sapap3*-KO mice (Piantadosi & Ahmari, unpublished observations). Given that 5-HT_{2C} receptors are selectively expressed on FSIs, these findings support our working hypothesis that increased activation of striatal FSIs can reduce behavioral compulsivity by reducing overall striatal gain and points toward 5-HT_{2C} receptors as clinically relevant targets for future drug developments.

Interestingly, the results of the present study indicate that overall striatal hyperactivity in *Sapap3*-KO mice is not driven by hyperactivity of D1 receptor-expressing SPNs. In fact, D1-SPNs were hypoactive at grooming onset in *Sapap3*-KO mice relative to WT littermates. While it is necessary to perform *in vivo* calcium imaging in A2A-cre *Sapap3*-KOs and WTs before making any strong assertions, as it currently stands, it appears that D1-SPNs play a smaller role in driving compulsive grooming in *Sapap3*-KO mice than expected. The findings in this translational model could potentially shift our current understanding of the neural mechanisms underlying compulsive symptoms of OCD patients and how we might optimize pharmacologic treatments to increase their effectiveness. Specifically, these data suggest that developing drugs that can specifically influence individual cell-types could yield greater clinical outcomes. As with any translational research, the impact of the results presented in this thesis must be viewed through a critical lens. However, the

present findings provide potentially relevant insights into the circuit level mechanisms underlying compulsive behaviors and the mechanisms by which SSRI treatment effectively reduces them.

BIBLIOGRAPHY

Ahmari, S. E., T. Spellman, N. L. Douglass, M. A. Kheirbek, H. B. Simpson, K. Deisseroth, J. A. Gordon, and R. Hen. 2013. 'Repeated Cortico-Striatal Stimulation Generates Persistent OCD-Like Behavior', 340: 1234-39.

Barr LC, Goodman WK, McDougle CJ, Delgado PL, Heninger GR, Charney DS, Price LH. 1994. 'Tryptophan depletion in patients with obsessive-compulsive disorder who respond to serotonin reuptake inhibitors', *Archives of General Psychiatry*, 51: 309-17.

Beaulieu, J. M., and R. R. Gainetdinov. 2011. 'The physiology, signaling, and pharmacology of dopamine receptors', *Pharmacol Rev*, 63: 182-217.

Berke, Joshua D. 2011. 'Functional Properties of Striatal Fast-Spiking Interneurons', 5.

Berney, A. et al. 2005. 'Lack of Effects on Core Obsessive-Compulsive Symptoms of Tryptophan Depletion During Symptom Provocation in Remitted Obsessive-Compulsive Disorder Patients ', *Biological psychiatry*, 59: 853-57.

Berridge, K. C., J. W. Aldridge, K. R. Houchard, and X. Zhuang. 2005. 'Sequential super-stereotypy of an instinctive fixed action pattern in hyper-dopaminergic mutant mice: a model of obsessive compulsive disorder and Tourette's', *BMC Biol*, 3: 4.

Blomeley, C. P., and E. Bracci. 2009. 'Serotonin excites fast-spiking interneurons in the striatum', *Eur J Neurosci*, 29: 1604-14.

Breiter, Hans C., Rauch, Scott L., Kwong, Kenneth K., Baker, John R., Weisskoff, Robert M., Kennedy, David N., Kendrick, Adair D., Davis, Timothy L., Jiang, Aiping, Cohen, Mark S., Stern, Chantal E., Belliveau, John W., Baer, Lee, O'Sullivan, Richard L., Savage, Cary R., Jenike, Michael A., Rosen, Bruce R. 1996. 'Functional Magnetic Resonance Imaging of Symptom Provocation in Obsessive-compulsive Disorder', *Archives of General Psychiatry*, 53: 595-606.

Burguiere, E., P. Monteiro, G. Feng, and A. M. Graybiel. 2013. 'Optogenetic Stimulation of Lateral Orbitofronto-Striatal Pathway Suppresses Compulsive Behaviors', *Science*, 340: 1243-46.

Chen, T. W., T. J. Wardill, Y. Sun, S. R. Pulver, S. L. Renninger, A. Baohan, E. R. Schreiter, R. A. Kerr, M. B. Orger, V. Jayaraman, L. L. Looger, K. Svoboda, and D. S. Kim. 2013. 'Ultrasensitive fluorescent proteins for imaging neuronal activity', *Nature*, 499: 295-300.

Christian, Christopher J., Todd Lencz, Delbert G. Robinson, Katherine E. Burdick, Manzar Ashtari, Anil K. Malhotra, Julia D. Betensky, and Philip R. Szeszko. 2008. 'Gray matter structural alterations in obsessive–compulsive disorder: Relationship to neuropsychological functions', 164: 123-31.

Corbit, V. L., E. E. Manning, A. H. Gittis, and S. E. Ahmari. 2019. 'Strengthened inputs from secondary motor cortex to striatum in a mouse model of compulsive behavior', *J Neurosci*.

Cui, G., S. B. Jun, X. Jin, M. D. Pham, S. S. Vogel, D. M. Lovinger, and R. M. Costa. 2013. 'Concurrent activation of striatal direct and indirect pathways during action initiation', *Nature*, 494: 238-42.

Deveney AM, Waddington JL. 1995. 'Pharmacological characterization of behavioral responses to SK&F 83959 in relation to 'D1-like' dopamine receptors not linked to adenylyl cyclase', *Journal of Pharmacology*, 116: 2120-26.

Gagnon, D., S. Petryszyn, M. G. Sanchez, C. Bories, J. M. Beaulieu, Y. De Koninck, A. Parent, and M. Parent. 2017. 'Striatal Neurons Expressing D1 and D2 Receptors are Morphologically Distinct and Differently Affected by Dopamine Denervation in Mice', *Sci Rep*, 7: 41432.

Ghosh, Kunal K., Laurie D. Burns, Eric D. Cocker, Axel Nimmerjahn, Yaniv Ziv, Abbas El Gamal, and Mark J. Schnitzer. 2011. 'Miniaturized integration of a fluorescence microscope', 8: 871-78.

Gittis, A. H., D. K. Leventhal, B. A. Fensterheim, J. R. Pettibone, J. D. Berke, and A. C. Kreitzer. 2011. 'Selective Inhibition of Striatal Fast-Spiking Interneurons Causes Dyskinesias', *Journal of Neuroscience*, 31: 15727-31.

Gittis, A. H., A. B. Nelson, M. T. Thwin, J. J. Palop, and A. C. Kreitzer. 2010. 'Distinct roles of GABAergic interneurons in the regulation of striatal output pathways', *J Neurosci*, 30: 2223-34.

Goddard, Andrew W., Anantha Shekhar, Aaron F. Whiteman, and Christopher J. McDougle. 2008. 'Serotoninergic mechanisms in the treatment of obsessive–compulsive disorder', *Drug Discovery Today*, 13: 325-32.

Graybiel, Ann M., and Scott L. Rauch. 2000. 'Toward a Neurobiology of Obsessive-Compulsive Disorder', 28: 343-47.

Harrison, Ben J., Carles Soriano-Mas, Jesus Pujol, Hector Ortiz, Marina López-Solà, Rosa Hernández-Ribas, Joan Deus, Pino Alonso, Murat Yücel, Christos Pantelis, José M. Menchon, and Narcís Cardoner. 2009. 'Altered Corticostriatal Functional Connectivity in Obsessive-compulsive Disorder', *Archives of General Psychiatry*, 66: 1189.

Jimenez, J. C., K. Su, A. R. Goldberg, V. M. Luna, J. S. Biane, G. Ordek, P. Zhou, S. K. Ong, M. A. Wright, L. Zweifel, L. Paninski, R. Hen, and M. A. Kheirbek. 2018. 'Anxiety Cells in a Hippocampal-Hypothalamic Circuit', *Neuron*, 97: 670-83 e6.

Kalanithi, P. S., W. Zheng, Y. Kataoka, M. DiFiglia, H. Grantz, C. B. Saper, M. L. Schwartz, J. F. Leckman, and F. M. Vaccarino. 2005. 'Altered parvalbumin-positive neuron distribution in basal ganglia of individuals with Tourette syndrome', *Proc Natl Acad Sci U S A*, 102: 13307-12.

Kalueff, Allan V., Adam Michael Stewart, Cai Song, Kent C. Berridge, Ann M. Graybiel, and John C. Fentress. 2015. 'Neurobiology of rodent self-grooming and its value for translational neuroscience', 17: 45-59.

Kataoka, Y., P. S. Kalanithi, H. Grantz, M. L. Schwartz, C. Saper, J. F. Leckman, and F. M. Vaccarino. 2010. 'Decreased number of parvalbumin and cholinergic interneurons in the striatum of individuals with Tourette syndrome', *J Comp Neurol*, 518: 277-91.

Kim, Jae-Jin, Lee, Myung Chul, Kim, Jaeseok, Kim, In Young, Kim, Sun I., Han, Moon Hee, Chang, Kee-Hyun, Kwon, Jun Soo 2001. 'Grey matter abnormalities in obsessive-compulsive disorder', *British Journal of Psychiatry*, 179: 330-34

.

Klapoetke, N. C., Y. Murata, S. S. Kim, S. R. Pulver, A. Birdsey-Benson, Y. K. Cho, T. K. Morimoto, A. S. Chuong, E. J. Carpenter, Z. Tian, J. Wang, Y. Xie, Z. Yan, Y. Zhang, B. Y. Chow, B. Surek, M. Melkonian, V. Jayaraman, M. Constantine-Paton, G. K. Wong, and E. S. Boyden. 2014. 'Independent optical excitation of distinct neural populations', *Nat Methods*, 11: 338-46.

Kravitz, A. V., B. S. Freeze, P. R. Parker, K. Kay, M. T. Thwin, K. Deisseroth, and A. C. Kreitzer. 2010. 'Regulation of parkinsonian motor behaviours by optogenetic control of basal ganglia circuitry', *Nature*, 466: 622-6.

Lee, K., S. M. Holley, J. L. Shobe, N. C. Chong, C. Cepeda, M. S. Levine, and S. C. Masmanidis. 2017. 'Parvalbumin Interneurons Modulate Striatal Output and Enhance Performance during Associative Learning', *Neuron*, 93: 1451-63 e4.

Maia, T. V., R. E. Cooney, and B. S. Peterson. 2008. 'The neural bases of obsessive-compulsive disorder in children and adults', *Dev Psychopathol*, 20: 1251-83.

Manning, Elizabeth E., Alexandre Y. Dombrovski, Mary M. Torregrossa, and Susanne E. Ahmari. 2018. 'Impaired instrumental reversal learning is associated with increased medial prefrontal cortex activity in Sapap3 knockout mouse model of compulsive behavior', *Neuropsychopharmacology*.

Mattheisen, M., J. F. Samuels, Y. Wang, B. D. Greenberg, A. J. Fyer, J. T. McCracken, D. A. Geller, D. L. Murphy, J. A. Knowles, M. A. Grados, M. A. Riddle, S. A. Rasmussen, N. C. McLaughlin, E. L. Nurmi, K. D. Askland, H. D. Qin, B. A. Cullen, J. Piacentini, D. L. Pauls, O. J. Bienvenu, S. E. Stewart, K. Y. Liang, F. S. Goes, B. Maher, A. E. Pulver, Y. Y. Shugart, D. Valle, C. Lange, and G. Nestadt. 2015. 'Genome-wide association study in obsessive-compulsive disorder: results from the OCGAS', *Mol Psychiatry*, 20: 337-44.

McCabe, C., Z. Mishor, N. Filippini, P. J. Cowen, M. J. Taylor, and C. J. Harmer. 2011. 'SSRI administration reduces resting state functional connectivity in dorso-medial prefrontal cortex', *Mol Psychiatry*, 16: 592-4.

Menzies, Lara, Samuel R. Chamberlain, Angela R. Laird, Sarah M. Thelen, Barbara J. Sahakian, and Ed T. Bullmore. 2008. 'Integrating evidence from neuroimaging and

neuropsychological studies of obsessive-compulsive disorder: The orbitofronto-striatal model revisited', *Neuroscience & Biobehavioral Reviews*, 32: 525-49.

Moresco, Rosa Maria, Lucia Pietra, Marta Henin, Andrea Panzacchi, Marco Locatelli, Lorena Bonaldi, Assunta Carpinelli, Clara Gobbo, Laura Bellodi, Daniela Perani, and Ferruccio Fazio. 2007. 'Fluvoxamine Treatment and D2 Receptors: a Pet Study on OCD Drug-Naïve Patients', 32: 197-205.

O'Hare, J. K., K. K. Ade, T. Sukharnikova, S. D. Van Hooser, M. L. Palmeri, H. H. Yin, and N. Calakos. 2016. 'Pathway-Specific Striatal Substrates for Habitual Behavior', *Neuron*, 89: 472-9.

Owen, S. F., J. D. Berke, and A. C. Kreitzer. 2018. 'Fast-Spiking Interneurons Supply Feedforward Control of Bursting, Calcium, and Plasticity for Efficient Learning', *Cell*, 172: 683-95 e15.

Page SJ, Terry P. 1997. 'Conditioned grooming induced by the dopamine D1-like receptor agonist SKF 38393 in rats.', *Pharmacol Biochem Behav.*, 57: 829-33.

Pauls, D. L., A. Abramovitch, S. L. Rauch, and D. A. Geller. 2014. 'Obsessive-compulsive disorder: an integrative genetic and neurobiological perspective', *Nat Rev Neurosci*, 15: 410-24.

Pennartz, C. M., J. D. Berke, A. M. Graybiel, R. Ito, C. S. Lansink, M. van der Meer, A. D. Redish, K. S. Smith, and P. Voorn. 2009. 'Corticostriatal Interactions during Learning, Memory Processing, and Decision Making', *J Neurosci*, 29: 12831-8.

Piras, F., F. Piras, C. Chiapponi, P. Girardi, C. Caltagirone, and G. Spalletta. 2015. 'Widespread structural brain changes in OCD: a systematic review of voxel-based morphometry studies', *Cortex*, 62: 89-108.

Pnevmatikakis, E. A., D. Soudry, T. A. Machado Y. Gao, D. Pfau J. Merel, Y. Mu T. Reardon, C. Lacefield, W. Yang, R. Bruno M. Ahrens, T. M. , D. S. Peterka Jessell, and L. Paninski R. Yuste. 2016. 'Simultaneous Denoising, Deconvolution, and Demixing of Calcium Imaging Data', 89: 285-99.

Pujol, Jesús, Carles Soriano-Mas, Pino Alonso, Narcís Cardoner, José M. Menchón, Joan Deus, and Julio Vallejo. 2004. 'Mapping Structural Brain Alterations in Obsessive-Compulsive Disorder', 61: 720.

Rauch, S., Jenike, M., Alpert, N., Baer, L., Breiter, H., Savage, C., Fischman, A. 1994. 'Regional Cerebral Blood Flow Measured During Symptom Provocation in Obsessive-Compulsive Disorder Using Oxygen 15-Labeled Carbon Dioxide and Positron Emission Tomography', *Archives of General Psychiatry*, 51: 62-70.

Resendez, S. L., J. H. Jennings, R. L. Ung, V. M. Namboodiri, Z. C. Zhou, J. M. Otis, H. Nomura, J. A. McHenry, O. Kosyk, and G. D. Stuber. 2016. 'Visualization of cortical, subcortical and deep brain neural circuit dynamics during naturalistic mammalian behavior with head-mounted microscopes and chronically implanted lenses', *Nat Protoc*, 11: 566-97.

Rotge, J. Y., D. Guehl, B. Dilharreguy, J. Tignol, B. Bioulac, M. Allard, P. Burbaud, and B. Aouizerate. 2009. 'Meta-analysis of brain volume changes in obsessive-compulsive disorder', *Biol Psychiatry*, 65: 75-83.

Rothwell, P. E., S. J. Hayton, G. L. Sun, M. V. Fuccillo, B. K. Lim, and R. C. Malenka. 2015. 'Input- and Output-Specific Regulation of Serial Order Performance by Corticostriatal Circuits', *Neuron*, 88: 345-56.

Saxena, S. 1998. 'Neuroimaging and frontal-subcortical circuitry in obsessive-compulsive disorder', *British Journal of Psychiatry*, 173: 26-37.

———. 1999. 'Localized Orbitofrontal and Subcortical Metabolic Changes and Predictors of Response to Paroxetine Treatment in Obsessive-Compulsive Disorder', 21: 683-93.

Sheintuch, L., A. Rubin, N. Brande-Eilat, N. Geva, N. Sadeh, O. Pinchasof, and Y. Ziv. 2017. 'Tracking the Same Neurons across Multiple Days in Ca(2+) Imaging Data', *Cell Rep*, 21: 1102-15.

Shepherd, G. M. 2013. 'Corticostriatal connectivity and its role in disease', *Nat Rev Neurosci*, 14: 278-91.

Shmelkov, S. V., A. Hormigo, D. Jing, C. C. Proenca, K. G. Bath, T. Milde, E. Shmelkov, J. S. Kushner, M. Baljevic, I. Dincheva, A. J. Murphy, D. M. Valenzuela, N. W. Gale, G. D. Yancopoulos, I. Ninan, F. S. Lee, and S. Rafii. 2010. 'Slitrk5 deficiency impairs corticostriatal circuitry and leads to obsessive-compulsive-like behaviors in mice', *Nat Med*, 16: 598-602, 1p following 02.

Smith, K. S., A. Virkud, K. Deisseroth, and A. M. Graybiel. 2012. 'Reversible online control of habitual behavior by optogenetic perturbation of medial prefrontal cortex', *Proc Natl Acad Sci U S A*, 109: 18932-7.

Stewart, S. E., D. Yu, J. M. Scharf, B. M. Neale, J. A. Fagerness, C. A. Mathews, P. D. Arnold, P. D. Evans, E. R. Gamazon, L. K. Davis, L. Osiecki, L. McGrath, S. Haddad, J. Crane, D. Hezel, C. Illman, C. Mayerfeld, A. Konkashbaev, C. Liu, A. Pluzhnikov, A. Tikhomirov, C. K. Edlund, S. L. Rauch, R. Moessner, P. Falkai, W. Maier, S. Ruhrmann, H. J. Grabe, L. Lennertz, M. Wagner, L. Bellodi, M. C. Cavallini, M. A. Richter, E. H. Cook, Jr., J. L. Kennedy, D. Rosenberg, D. J. Stein, S. M. Hemmings, C. Lochner, A. Azzam, D. A. Chavira, E. Fournier, H. Garrido, B. Sheppard, P. Umana, D. L. Murphy, J. R. Wendland, J. Veenstra-VanderWeele, D. Denys, R. Blom, D. Deforce, F. Van Nieuwerburgh, H. G. Westenberg, S. Walitza, K. Egberts, T. Renner, E. C. Miguel, C. Cappi, A. G. Hounie, M. Conceicao do Rosario, A. S. Sampaio, H. Vallada, H. Nicolini, N. Lanzagorta, B. Camarena, R. Delorme, M. Leboyer, C. N. Pato, M. T. Pato, E. Voyiaziakis, P. Heutink, D. C. Cath, D. Posthuma, J. H. Smit, J. Samuels, O. J. Bienvenu, B. Cullen, A. J. Fyer, M. A. Grados, B. D. Greenberg, J. T. McCracken, M. A. Riddle, Y. Wang, V. Coric, J. F. Leckman, M. Bloch, C. Pittenger, V. Eapen, D. W. Black, R. A. Ophoff, E. Strengman, D. Cusi, M. Turiel, F. Frau, F. Macciardi, J. R. Gibbs, M. R. Cookson, A. Singleton, Consortium North American Brain Expression, J. Hardy, U. K. Brain Expression Database, A. T. Crenshaw, M. A. Parkin, D. B. Mirel, D. V. Conti, S. Purcell, G. Nestadt, G. L.

Hanna, M. A. Jenike, J. A. Knowles, N. Cox, and D. L. Pauls. 2013. 'Genome-wide association study of obsessive-compulsive disorder', *Mol Psychiatry*, 18: 788-98.

Stoessl, AJ. 1994. 'Dopamine D1 receptor agonist-induced grooming is blocked by the opioid receptor antagonist naloxone.', *Eur J Pharmacology*, 259: 301-03.

Surmeier, D. James, Jun Ding, Michelle Day, Zhongfeng Wang, and Weixing Shen. 2007. 'D1 and D2 dopamine-receptor modulation of striatal glutamatergic signaling in striatal medium spiny neurons', 30: 228-35.

Svenningsson, P., A. Nishi, G. Fisone, J. A. Girault, A. C. Nairn, and P. Greengard. 2004. 'DARPP-32: an integrator of neurotransmission', *Annu Rev Pharmacol Toxicol*, 44: 269-96.

Taylor, S. 2011. 'Etiology of obsessions and compulsions: a meta-analysis and narrative review of twin studies', *Clin Psychol Rev*, 31: 1361-72.

van de Ven, V., M. Wingen, K. P. Kuypers, J. G. Ramaekers, and E. Formisano. 2013. 'Escitalopram Decreases Cross-Regional Functional Connectivity within the Default-Mode Network', *PLoS ONE*, 8: e68355.

Van Den Heuvel, O. A., P. L. Remijnse, D. Mataix-Cols, H. Vrenken, H. J. Groenewegen, H. B. M. Uylings, A. J. L. M. Van Balkom, and D. J. Veltman. 2008. 'The major symptom dimensions of obsessive-compulsive disorder are mediated by partially distinct neural systems', *Brain*, 132: 853-68.

Wan, Y., K. K. Ade, Z. Caffall, M. Ilcim Ozlu, C. Eroglu, G. Feng, and N. Calakos. 2014. 'Circuit-selective striatal synaptic dysfunction in the Sapap3 knockout mouse model of obsessive-compulsive disorder', *Biol Psychiatry*, 75: 623-30.

Wan, Y., G. Feng, and N. Calakos. 2011. 'Sapap3 deletion causes mGluR5-dependent silencing of AMPAR synapses', *J Neurosci*, 31: 16685-91.

Welch, Jeffrey M., Jing Lu, Ramona M. Rodriguiz, Nicholas C. Trotta, Joao Peca, Jin-Dong Ding, Catia Feliciano, Meng Chen, J. Paige Adams, Jianhong Luo, Serena M. Dudek, Richard J. Weinberg, Nicole Calakos, William C. Wetsel, and Guoping Feng. 2007. 'Cortico-striatal synaptic defects and OCD-like behaviours in Sapap3-mutant mice', *Nature*, 448: 894-900.

Xu, M., L. Li, and C. Pittenger. 2016. 'Ablation of fast-spiking interneurons in the dorsal striatum, recapitulating abnormalities seen post-mortem in Tourette syndrome, produces anxiety and elevated grooming', *Neuroscience*, 324: 321-29.

Zalocusky, K., Ramakrishnan, C., Lerner, T., Davidson, T., Knutson, B., Deisseroth, K. 2016. 'Nucleus accumbens D2R cells signal prior outcomes and control risky decision-making', *Nature*, 531: 642-46.

Zhong, Ping, and Zhen Yan. 2011. 'Differential Regulation of the Excitability of Prefrontal Cortical Fast-Spiking Interneurons and Pyramidal Neurons by Serotonin and Fluoxetine', 6: e16970.

Zhou, P., S. L. Resendez, J. Rodriguez-Romaguera, J. C. Jimenez, S. Q. Neufeld, A. Giovannucci, J. Friedrich, E. A. Pnevmatikakis, G. D. Stuber, R. Hen, M. A. Kheirbek, B. L. Sabatini, R. E. Kass, and L. Paninski. 2018. 'Efficient and accurate extraction of in vivo calcium signals from microendoscopic video data', *Elife*, 7.